Developing a Local Characterization Procedure to Study the Dielectric Properties of HfO_2 on MoS_2

A thesis presented in partial fulfillment of the requirements for the degree of Bachelor of Arts in Physics with Honors

Beatrice Croteau

B.A. Degree Candidate in Physics

Faculty Advisor: Katherine Aidala

Mount Holyoke College

South Hadley MA

May 12, 2026

Contents

List of Figures iv

1 Introduction 2

1.1 Dielectrics and Transistors 2

1.1.1 Dielectric Scaling Options 4

1.2 2D Semiconductor Materials 6

1.2.1 Transition Metal Dichalcogenides (TMDs) 7

1.2.2 High-k Dielectric and 2D TMD Integration 7

1.3 Dielectric Characterization 8

1.3.1 Bulk Parameter Extraction Methods 9

1.3.2 Defect Characterization Methods 9

1.4 Prior Charge Diffusion Work 11

1.5 Summary and Outline of the Thesis 16

2 Methods 18

2.1 Sample Fabrication 18

2.2 Atomic Force Microscopy 20

2.2.1 Basic Principles 20

2.2.2 Kelvin Probe Force Microscopy 22

2.3 Charge Diffusion Measurements 24

2.3.1 Sample Holder 24

2.3.2 Environmental Controls . . . 25
2.3.3 Charge Injection . . . 26
2.3.4 Diffusion Measurements . . . 27

3 Results and Analysis **29**
3.1 Initial Experiments: The Importance of Environmental Control . . . 29
3.1.1 Ambient Conditions . . . 30
3.1.2 In Nitrogen . . . 32
3.1.3 Pre-Injection Heating . . . 33
3.2 Diffusion at Elevated Temperatures . . . 36

4 Discussion and Future Work **42**
4.1 Charge Diffusion Models . . . 44
4.2 Future Work . . . 46

A Charge Diffusion Procedure **48**
A.1 The Night Before Imaging . . . 48
A.1.1 Sample Setup . . . 48
A.1.2 Tuning Setup . . . 49
A.1.3 AC Topography Scan . . . 49
A.1.4 KPFM Test . . . 50
A.1.5 Injection Test . . . 51
A.1.6 Measure CPD . . . 53
A.1.7 Flowing Nitrogen . . . 54
A.2 The Day of Imaging . . . 54
A.2.1 Heating the Sample . . . 54
A.2.2 Charge Injection . . . 56
A.2.3 Sample Heating II . . . 57
A.2.4 KPFM . . . 58

Bibliography **59**

List of Figures

1.1 A schematic for a thin-film MOSFET. Metals are in blue, insulators in orange, and semiconductors in green. The metal, dielectric, and semiconductor form a capacitor. A voltage V_G is applied to the metal, creating an electric field between metal and semiconductor, inducing a channel between source and drain. . . . 4

1.2 a. Atomic structure of MoS_2 [1] b. Optical image of an MoS_2 flake. [2] . . . 8

1.3 Surface potential at the charge accumulation site in a 30 Å HfO_2/10 Å SiO_2 sample over time for different queue times. Queue time is the time between oxide deposition and the surface voltage measurement. Measurements were taken in ambient conditions [3]. . . . 10

1.4 Contact Potential Difference (CPD) measurements over time made by KPFM of two charge injection spots in the HfO_2 layer of an HfO_2/p-Ge/p-Si sample. The inset images are KPFM images of the injection spot at selected times[4]. 12

1.5 a. Lateral size (full width at the half-maximum value) of an injection spot in ambient conditions (squares) and in vacuum (circles) over time. We can see that the lateral spreading of the injection site is greatly increased in vacuum compared to ambient conditions. b. Lateral size squared over time for injection in SiO_2 (full squares) and Si_3N_4 (full and open triangles represent two different experimental runs). . . . 15

1.6 Natural log of the diffusion coefficient plotted against $\frac{1}{k_b T}$. The slope of this line is the trap activation energy[5] 16

2.1 Optical microscope image of the sample after MoS_2 flakes have been exfoliated on the silicon wafer, prior to HfO_2 deposition. The silicon wafer shows up orange in the image, and the flakes are varying shades of brown. 19

2.2 a. Basic AFM AC Tapping Mode setup. Relevant setup components are labeled. b. AC Tapping Mode image of our sample, showing one MoS_2 flake over the silicon substrate. The brighter sections of the image are the flake. The tallest region of the flake is at the bottom of the image, and each darker plateau on the flake signifies a region with fewer MoS_2 monolayers. 21

2.3 AFM KPFM setup. All physical components are the same as those in the diagram for AC Tapping Mode. 22

2.4 a. Topographic image produced during a KPFM scan of our sample. b. Surface potential image produced during a KPFM scan of our sample. We can see how topography aligns with the potential measurements: the bright line through the middle of the image is the edge of a flake on the sample surface. 23

2.5 Picture of the sample mounted on its sample holder. The BNC connection to ground and plastic tube for nitrogen are labeled. The grounding BNC is connected through a wire and conducting clip to a metal puck. 24

2.6 a. Tip holder with the flexible black membrane attached. A tip is mounted on the tip holder. b. Tip holder and sample holder in place for an AFM measurement. The tip holder is held blue side-down over the sample holder, creating a loose seal of the tip-sample system. 25

2.7 a. Example KPFM potential image with a line slice drawn through it. b. Plot of the line slice. The horizontal slice averages over 100 nm. 28

3.1 a. A grid of injection points 33 minutes after injection. in ambient conditions. b. The grid of injection points 61 minutes after injection. 30

3.2 CPD over time in ambient conditions for different injection parameters. The measurements for -3V, 60s and -4V, 10s are missing due to poor positioning of the scan window missing the injection locations for multiple KPFM runs resulting in only two data points for each. 31

3.3 Potential image taken during KPFM monitoring of the charge diffusion experiment in a dry nitrogen environment with no sample heating. The injection parameters for each charge injection spot is labeled. 32

3.4 a. Maximum CPD of each injection spot with reference to the background for all positive injection voltages at select times. b. Maximum magnitude of CPD of each injection spot with reference to the background for all negative injection voltages at select times. 33

3.5 Potential image produced during KPFM scanning of the surface of the $HfO_2/MoS_2/Si$ sample following charge injection at 6V for two minutes. The sample was left in nitrogen for 10 hours and heated to 150°C for 15 minutes prior to injection. 35

3.6 a. Maximum CPD value at each injection spot measured in reference to the background potential value over time. b. Charge density at each injection location over time. 35

3.7 Potential image taken during KPFM scannning of the $HfO_2/MoS_2/Si$ sample following charge injection at 4V for two minutes. The sample was left in nitrogen for 10 hours and heated to 150°C for 15 minutes prior to injection. Injection was performed at 70°C, and diffusion measurements were taken at 90°C. 37

3.8 Maximum CPD over time for 4V, 2 minute injections in HfO_2 on MoS_2 and Si. 38

3.9 On the left axis is the maximum CPD and on the right axis is charge density. Both are plotted against time for the injection spots on and off the MoS_2 flake. Each data point can be read on both axes, on the left for its CPD value and on the right for its charge density. An exponential decay was fit to both series of CPD data. 39

3.10 a. CPD profiles at select times during charge diffusion measurements on an MoS_2 flake. b. Integrated CPD line profiles over time during charge diffusion measurements on an MoS_2 flake. 40

A.1 Example deflection vs. z-sensor force curve. 52

Abstract

The semiconductor industry will eventually run up against the limits of silicon field-effect transistors. Ultrathin transition metal dichalcogenides (TMDs) are promising candidates to enable continued scaling of microelectronics, beyond the limits of silicon. This will require methods to integrate TMDs with high-performance dielectric materials. Hafnium oxide (HfO_2), a well-studied high-k dielectric, is a promising candidate for integration with TMDs in novel transistor technology. There is not yet an established process for this integration due to challenges arising from the dissimlar chemistry of TMD surfaces and ALD oxides. We use Atomic Force Microscopy (AFM) to study the integration of HfO_2 grown by Plasma-Enhanced ALD with the 2D TMD MoS_2 through charge diffusion measurements, a form of local defect characterization. We have developed a procedure for these measurements in which we inject charge into the exposed oxide surface using the AFM tip, and then use Kelvin Probe Force Microscopy (KPFM) to measure changes in surface potential over time as the injected charge leaks through the thin oxide layer. This procedure was developed with careful consideration of how the measurement environment impacts these electrical measurements. This approach enables quantitative comparison of dielectric performance of oxides on the nanoscale, akin to industry-established methods of wafer-scale oxide integrity testing, which will inform our evaluation of the integration between HfO_2 and MoS_2.

Acknowledgements

Writing this thesis was a fulfilling challenge for my senior year, but completing it would not have been possible without support from my professors, family, and friends.

I would like to begin by thanking Professor Kathy Aidala, my research advisor since my first year at MHC. Kathy has been an incredible mentor and advisor for the past three years. Thank you for taking the time to teach me, give me meaningful feedback, and push me to be a better researcher. I would also like to thank the rest of my thesis committee, Professor Kerstin Nordstrom and Professor Lidia Mrad, for taking the time to read my thesis and provide feedback. Thank you also for your support as my professors throughout my time at Mount Holyoke. I extend a major thank you to our collaborators, Rafael Jaramillo and Rishabh Kothari, who fabricated the samples used in this work and provided useful insight in our conversations about charge diffusion measurements.

Thank you to the Mount Holyoke Physics Department as a whole for making my physics studies at Mount Holyoke so rewarding and fun. A special shout-out to the two people that keep this department running: Rob Higley (who can fix anything) and Loryn Engelbrecht (herding the cats–physicists–of this department is a difficult but necessary job).

Thank you to my family and friends for their support through the thesis-writing process and for listening to me talk about atomic force microscopy for the past three years.

Lastly, an anti-acknowledgment to my Physics-250 TA students: I would've gotten a lot more thesis editing done on Wednesday and Thursday nights if you all had asked me less questions.

Chapter 1

Introduction

In this thesis, we present the development of a procedure for the measurement and analysis of charge diffusion in the oxide HfO_2 as a method to evaluate its integration with the 2D semiconductor MoS_2. To understand the significance of these measurements, this chapter will discuss the use of HfO_2 and other high-k dielectrics in novel transistor technology, the importance of characterizing the integration between dielectrics and semiconductors for transistor development, and the methods through which this characterization can be performed. We will also discuss the prior characterization work upon which the experimental and analytic methods of this thesis are built.

1.1 Dielectrics and Transistors

Transistors are one of the most significant technological developments of the last century. They are an integral part of modern electronic devices, and the development of novel transistors is an area of active study. Innovations in transistor technology necessarily require the characterization of dielectric and semiconductor materials, two key components used in their fabrication.

Dielectrics are insulators, meaning they have a large energy band gap that discourages the flow of electrons through the material. Many different parameters can be used to describe

dielectric performance, including trap density, the diffusion coefficient, resistivity, and more. The key descriptor of a dielectric is its dielectric constant k, also known as the relative permittivity of a dielectric, where

$$k = \frac{\epsilon}{\epsilon_0}.$$

Here, ϵ_0 is the permittivity of free space and ϵ is the permittivity of the dielectric in question. The dielectric constant is an important descriptor of dielectric function because it determines, in tandem with dielectric thickness, the strength of the electric field that can be produced across a dielectric. Dielectrics are one of three types of materials needed in a transistor. In this work, we also focus on semiconductors, materials with mid-range energy band gaps, located in magnitude between those of insulators and conductors. This allows them to act as both a conductor and an insulator under different conditions. When placed in a large enough external electric field, electrons in semiconductors will gain the energy required to move up in atomic energy levels and move through the material, forming an electric current without damaging the material. When combined with a metal, dielectrics and semiconductors can form transistors.

First invented in Bell Laboratories in 1947, transistors revolutionized electronics, paving the way for the development of integrated circuits and microprocessors, as well as the miniaturization of this technology[6]. The metal-oxide- semiconductor field effect transistor (MOSFET), was first developed in 1960 at Bell Laboratories. It will serve as the technological motivation for the work presented in this thesis.

MOSFETs have three main layers: a metal, a semiconductor, and an oxide. As seen in Figure 1.1, the oxide is positioned between the metal and semiconductor layers. In addition to a metal layer, there are also two metal contacts in the semiconductor layer, called the source and drain. When a voltage V_G is applied to the metal layer of the MOSFET, an electric field is produced across the insulating layer, accounting for the "field-effect" portion of the MOSFET name. This electric field creates a build-up of charge in the semiconductor layer at its interface with the oxide. When V_G is greater than a threshold ("turn-on")

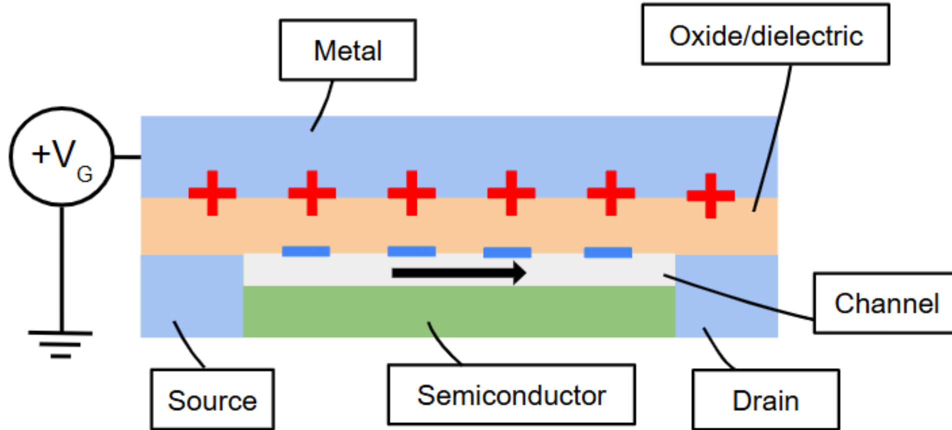

Figure 1.1: A schematic for a thin-film MOSFET. Metals are in blue, insulators in orange, and semiconductors in green. The metal, dielectric, and semiconductor form a capacitor. A voltage V_G is applied to the metal, creating an electric field between metal and semiconductor, inducing a channel between source and drain.

voltage determined by material properties of the MOSFET and a voltage is applied between the source and drain, the build-up of charges on the semiconductor allows charge to flow between the source and drain [7].

MOSFETs have traditionally been fabricated with a silicon-oxide (SiO_2) dielectric layer directly oxidized on top of a silicon (Si) semiconductor layer. Silicon is used for its availability, affordability, and easily-controlled purity. The direct oxidation of SiO_2 on Si layer yields a high quality interface ideal for transistor operation. As transistors are scaled down for improved speed and power consumption however, silicon is reaching its limits[7]. This limitation in silicon's material properties has led to the development and characterization of novel dielectrics and semiconductors as potential replacements and supplements to the present standards, allowing further innovation in the field of transistor technology.

1.1.1 Dielectric Scaling Options

Transistor scaling is governed by speed and power. Transistor speed, a measure of how many charges can be generated in the channel in a set period of time, is limited by dielectric thickness and the dielectric constant k. These dielectric parameters mediate a tradeoff

between transistor speed and power, as thinner dielectrics are better for transistor speed, but lose more power due to gate leakage current for a given dielectric constant. As SiO_2 decreases in thickness, electrons are able to tunnel through it, increasing the gate leakage current to the point that the SiO_2 layer ceases to function as a reliable dielectric [8]. This boundary for the scaling of SiO_2 requires that insulators with properties better suited for transistor scaling be sought out and characterized for transistor technology development.

There has been a move towards high-k dielectrics in the past few decades as they are able to be physically thicker with a large capacitance, which reduces tunneling leakage current while maintaining optimal capacitance characteristics. The relationship between capacitance, dielectric constant, and thickness is as follows:

$$C = \epsilon_0 k \frac{A}{d}, \tag{1.1}$$

where d is the dielectric thickness and A is the area of our region of interest [7]. When the dielectric constant k is large enough, a high capacitance can be maintained while insulator thickness increases. High capacitance is ideal for transistor performance because of the relationship between capacitance and surface charge. As capacitance increases, for the same voltage applied to the MOSFET gate, a larger number of charges will collect on either side of the dielectric, increasing the number of charges in the channel, which increases transistor speed. Maintaining a high capacitance even with a thick dielectric layer lowers the tunneling leakage current, which means less power is lost, and the transistor device is more efficient.

Proposed high-k dielectric replacements for SiO_2 in the MOSFET oxide layer include HfO_2, ZrO_2, Si_3N_4, Al_2O_3, and TiO_2. Of this list, HfO_2 is a promising candidate for dielectric replacement due to its high dielectric constant ($k = 25$) and well-understood growth behavior[9]. When formed through atomic layer deposition (ALD) on a semiconductor layer of silicon, HfO_2 yields a high performance dielectric layer with controllable morphology. The integration of HfO_2 with other semiconductor materials is an area of active research. In some areas, HfO_2 is already used as a silicon-oxide replacement in transistor devices. For

example, Intel Corporation began using HfO_2 as part of its 45 nm technology manufacturing process in 2007 [10]. The growth behavior of HfO_2 and its applications to areas including low-power devices and low-volatility memory have been previously studied [11][12]. While high-k metal-oxide dielectrics like HfO_2 reduce gate-leakage current with a physically thicker insulating layer, they may yield extended defects that provide paths for leakage current [13]. For high-k dielectrics to be a viable replacement for SiO_2 on an industry-wide level, the electrical properties of these materials must be studied, providing greater understanding of their defects and how to improve them.

1.2 2D Semiconductor Materials

To scale MOSFETs, their channel length must be shortened, which poses a challenge for silicon-based devices. Reducing channel length is directly related to increasing channel current flow and transistor switching speed, while reducing power consumption. When the channel length is shortened however, it becomes sensitive to the short channel effect. In MOSFET devices, after applying the voltage to the top metal layer, charges are induced along all the semiconductor interfaces. The charges at the interfaces with the source and drain are considered electrically "shared" between the top metal layer and source/drain. While most charges at the semiconductor interface generate electric fields that contribute to increasing the transistor threshold voltage, shared charges at the source and drain produce electric fields that terminate in the source and drain, and thus do not contribute to the threshold voltage. When the channel is shortened, these shared charges comprise a significant portion of the charges at the semiconductor interface due to the altered geometry, therefore significantly lowering the threshold voltage. Lowering the threshold voltage too far prevents precise control of transistor operation[7]. To address the short channel effect, the channel thickness can be reduced, allowing the gate voltage to accurately control channel functioning. As silicon is a 3D material however, reducing the channel to nanometer thicknesses inevitably

introduces surface roughness and defects. In turn, control over the channel current flow is reduced, which increases leakage current and power dissipation [14][15]. Two-dimensional materials make a promising replacement for three-dimensional semiconductors in transistors because they can form uniform, smooth, thin channels.

1.2.1 Transition Metal Dichalcogenides (TMDs)

Two-dimensional materials form discrete atomic layers, which have strong intermolecular bonds within layers and weaker Van der Waals bonds between layers. This structure yields atomically thin channels for transistor scaling, promising small, low-power devices with high gate controllability [15]. As opposed to three-dimensional materials, 2D materials have thin layers with smooth surfaces that lend themselves to nanometer-level scaling.

Transition-metal-dichalcogenides (TMDs) are a class of two-dimensional semiconductors under consideration for use in next-generation electronic devices. TMDs are formed with a single transition metal atom and two chalcogen atoms. They are of particular interest for their physical structure, which allows for precise control of band gap and charge carrier characteristics, which determine channel formation and quality in MOSFET devices [16]. TMDs are already used in lab-fabricated MOSFETs [17][18].

Molybdenum disulfide, MoS_2, is one of the most widely -studied 2D TMDs, with well-developed synthesis and exfoliation processes. Its crystal structure and physical appearance are shown in Figure 1.2. MoS_2 has multiple promising qualities, including a direct bandgap of about 1.8 eV in monolayer form and very good charge carrier mobility, making it a strong candidate for next-generation electronic devices.

1.2.2 High-k Dielectric and 2D TMD Integration

The material properties of high-k dielectrics and 2D TMD semiconductors suggest that they could eventually yield high-functioning MOSFET devices. There are however, numerous challenges to overcome in seeing these devices come to fruition. One such challenge is re-

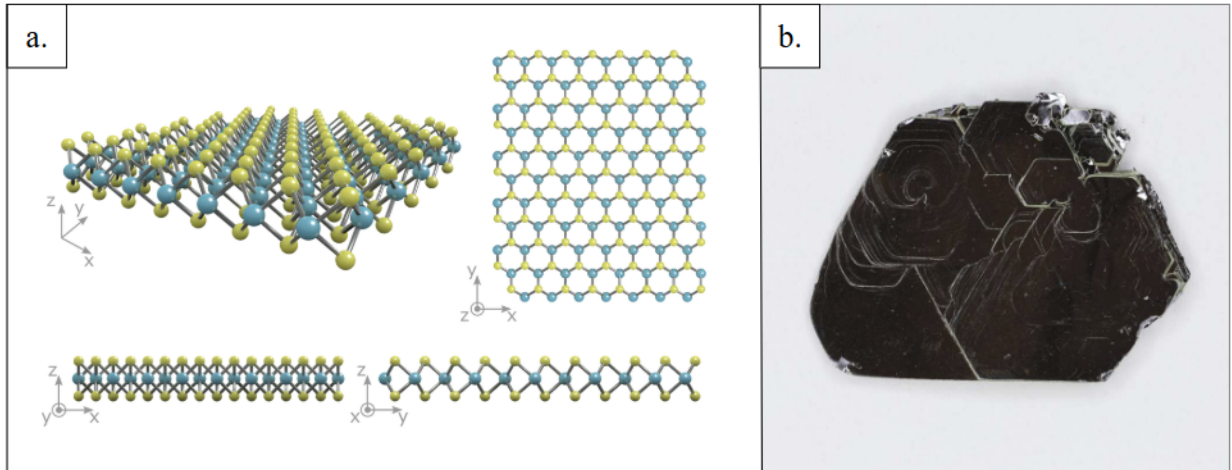

Figure 1.2: a. Atomic structure of MoS_2 [1] b. Optical image of an MoS_2 flake. [2]

placing the silicon/silicon-oxide based interface in transistors with a semiconductor-dielectric interface of comparable quality. Defects in the semiconductor-dielectric interface of MOSFET devices impact key device performance parameters, including the threshold voltage, speed, power consumption, and the drain current [19].

The Si/SiO_2 interface is comprised of a dielectric layer directly oxidized on top of the semiconductor layer. This yields a high-quality interface with fewer defects compared to other dielectric layer growth methods. As many of the proposed dielectric replacements for transistors do not include native oxides grown on the semiconductor layers, refinement of the growth techniques and characterization of the semiconductor/dielectric interface is of utmost importance [20]. Characterization of both the semiconductor and dielectric layers, and their interface, must be undertaken in order to understand and refine the integration of novel dielectric and semiconductor material combinations.

1.3 Dielectric Characterization

Evaluation of the performance of a dielectric will involve applying an electrical stress to the material and using the results to extract key material parameters. As mentioned in Section 1.1, dielectrics can be described by values like their dielectric constant, resistivity,

trap density, trap energy levels, and diffusion coefficient, among others. Some of these values can be extracted through the application of bulk electrical stress, while others require local defect characterization methods. For high-k dielectrics to be used on an industry-wide scale, their electrical properties, specifically their defects, need to be well-understood. The defects in dielectrics will also change based on their substrate material; even if only the dielectric is being characterized, the behavior of that dielectric layer changes depending on the material it's grown on. For that reason, we employ a local defect characterization method, charge diffusion analysis, in the experimental work of this thesis. Before discussing charge diffusion, we will outline several of the more common characterization techniques that can be used on dielectrics.

1.3.1 Bulk Parameter Extraction Methods

To extract general material properties, understand its insulating performance, and find the stress limits of dielectrics, bulk material characterization methods can be employed. For instance, current-voltage sweep experiments can yield measurements for the dielectric constant, gate leakage current, trap density, and trap energy levels [21][22]. For such measurements, the dielectric material is sandwiched between two conducting electrodes while a voltage applied across the material is swept through a range of values. The current measured through the material as a result of the applied voltage is recorded, providing dielectric information. This setup can also be used to perform impedance spectroscopy, in which an AC voltage is applied across the electrodes over a range of frequencies. Such measurements can yield values for capacitance and conductance of dielectric materials [23].

1.3.2 Defect Characterization Methods

Beyond bulk measurement techniques, more localized characterization can be done, providing higher resolution and greater detail about material heterogeneity. One such method is micro-corona-Kelvin characterization. Mirco-corona-Kelvin measurements bring a charged

probe 1-2 mm in diameter to the surface of a dielectric to deposit a known amount of ionic charge on the surface. By monitoring the diffusion of this charge, measurements of capacitance, work-function, and doping concentration can be acquired. Marinsky *et al.* presents micro-corona Kelvin characterization of HfO_2. After holding a probe above their 30 Å HfO_2/10 Å SiO_2 sample for enough time to achieve thorough charge accumulation, they recorded the change in surface potential at this charged site over time[3]. These measurements are displayed in Figure 1.3 below. The key dielectric measurements mentioned above were extracted from this information.

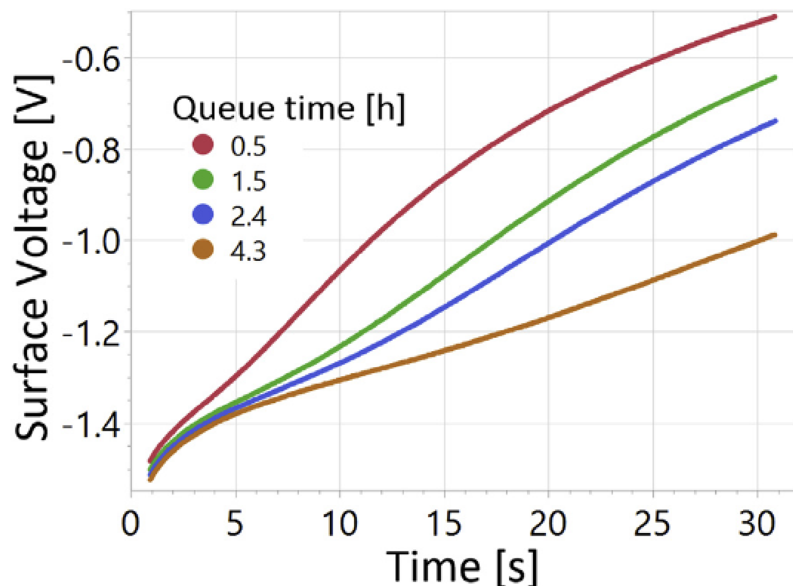

Figure 1.3: Surface potential at the charge accumulation site in a 30 Å HfO_2/10 Å SiO_2 sample over time for different queue times. Queue time is the time between oxide deposition and the surface voltage measurement. Measurements were taken in ambient conditions [3].

Aside from the micro-corona-Kelvin method, most local characterization is performed using Atomic Force Microscopy (AFM). Multiple AFM techniques can be used to characterize dielectrics, including electric force microscopy (EFM), Kelvin-probe force microscopy (KPFM), and conductive atomic force microscopy (CAFM). CAFM measurements are similar to bulk IV curve characterization methods, though the top electrode is now a movable AFM tip about four orders of magnitude smaller than the dielectric surface area. Taking

repeated CAFM measurements over a range of voltages and locations on a sample can provide statistical information about the quality of the dielectric and the prevalence of defects [24][25].

The EFM and KPFM methods both operate by scanning a biased AFM probe a set distance above the surface of the dielectric to gather information about electrical properties of the sample through an electric field generated between tip and surface. Dielectric characterization using EFM and KPFM typically involves charge diffusion measurements. In such measurements, an AFM probe is brought into contact with the surface, after which a voltage is applied for a set amount of time. This process injects charge into the dielectric sample. Local electrical measurements with EFM and KPFM can then be used to monitor the diffusion of this charge throughout the oxide through changes in the surface potential [26] [27] [28] [29] [30] [31] [32] [33] [5] [4] [34]. While EFM measurements provide only qualitative information about the diffusion of the injected charge over time, KPFM measurements yield quantitative information that with careful consideration of the physical system, can produce diffusion coefficients, trap activation energy, and charge density measurements, all of which tell us about the defects present in a dielectric sample and at the interface of the dielectric with its substrate. Further modifications of these techniques, like those in Kelvin Probe Force Gradient Microscopy, can possibly yield additional and/or more precise quantitative measurements [35]. We perform charge diffusion measurements with KPFM for the characterization presented in this thesis. In the following section, we will present the three most relevant prior papers upon which our experimental and analytical approaches are based.

1.4 Prior Charge Diffusion Work

Here we present the experimental overview and basic analytic techniques used in the most relevant prior work for our experimental methods. The models and procedures used in these papers informed the development of our experimental methods, including the dielectric

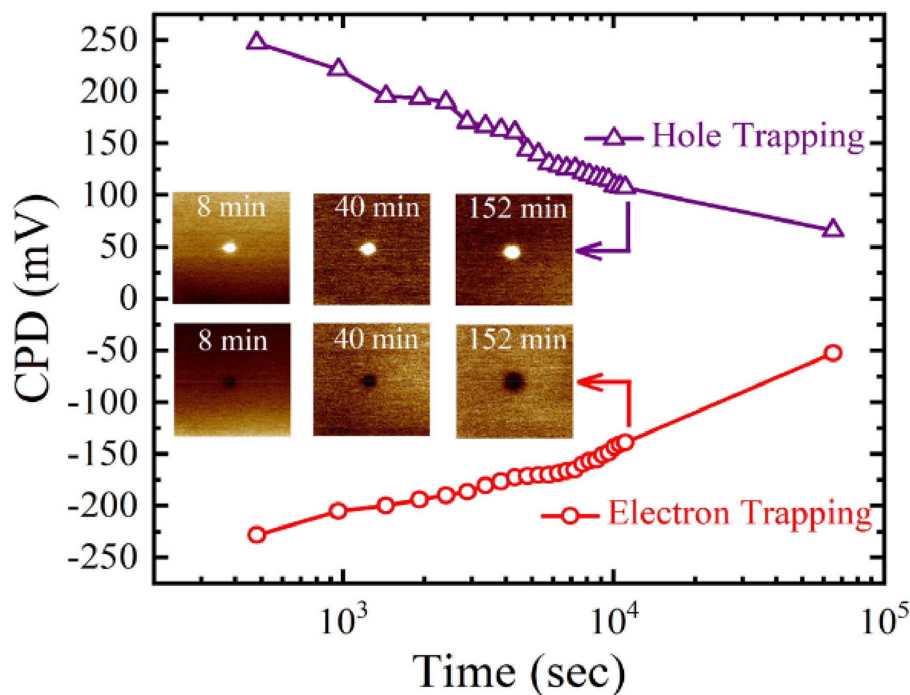

Figure 1.4: Contact Potential Difference (CPD) measurements over time made by KPFM of two charge injection spots in the HfO_2 layer of an HfO_2/p-Ge/p-Si sample. The inset images are KPFM images of the injection spot at selected times[4].

characterization parameters we extracted or hope to extract in the future: charge density, diffusion coefficient, and trap activation energy.

Choudary *et al.* performed charge diffusion measurements on an HfO_2/p-Ge/p-Si sample. The AFM probe was biased to -3 V and +3 V to inject electrons and holes respectively into the HfO_2 layer. Their charge diffusion measurements were taken using KPFM. We can see the change over time in their contact potential difference (CPD) between tip and sample in Figure 1.4, measurements which were extracted from KPFM measurements at the charge injection locations[4].

Using the CPD information over time from Figure 1.4 and modeling the sample/tip system as a parallel plate capacitor, they were able to make a calculation of charge density for each step in time. The parallel plate model assumes that the tip and substrate function as a parallel plate capacitor with two dielectrics in between: the air between tip and sample,

and the oxide layer. This relationship is described by the following equation,

$$N = \frac{\epsilon_0 V_{CPD}}{q[\frac{t_{air}}{\epsilon_{air}} + \frac{t_{ox}}{\epsilon_{ox}}]} \tag{1.2}$$

where N is the density of charges, ϵ_0 is the permittivity of free space, V_{CPD} is the potential of the charge spot, q is the charge, t_{air} is the separation distance between tip and surface, ϵ_{air} is the relative permittivity of air, t_{ox} is the thickness of the oxide, and ϵ_{ox} is the relative permittivity of the oxide layer. Making this calculation of charge density for different points in time gives us information about how much charge is held within the oxide layer, and how that changes over time, i.e. how charge is diffusing through the dielectric. A model for the specific mechanics by which charge moves is discussed in the following section.

Dunaevskiy *et al.* and Knorr *et al.* both present the following description for charge diffusion through a dielectric. Charge diffuses in two primary directions, lateral and vertical, and through two mechanisms: electrostatic Coulomb repulsion of like charges and diffusive motion of charges through traps. In this case, the term diffusion is describing a random walk by charges through traps in the dielectric. Traps are potential energy wells within the dielectric structure where free charges (electrons) can become stuck, unable to move until more energy is provided for them to escape. Coulomb repulsion likely accounts for the initial diffusive behavior, when there is a large number of like charges in close proximity. On a longer time scale however, random movement through traps becomes the main driver of diffusion as charges get further apart. The time scale on which we are able to measure diffusion with KPFM means that we miss the Coulombic repulsion and only measure the effects of diffusion through traps. The comparative levels of vertical and lateral diffusion can be inferred from the amount of lateral spreading of charge in the oxide over time compared to the amount that the total charge measured by KPFM in the oxide reduces over time [36][35].

Dunaevskiy *et al.* uses measurements of lateral charge spreading to extract the diffusion coefficient of an SiO_2 oxide in their samples. The diffusion coefficient is a value used to

quantify the rate of diffusion. For our purposes, the diffusion coefficient has units of cm^2 per second to describe the rate of charge diffusion. Here, researchers injected charge using an AFM probe biased to -4 V on a sample with a 10-nm thick SiO_2 dielectric layer embedded with silicon nano-crystals. After injection, they took measurements of the width of the injection spot on each KPFM potential image. They applied the one-dimensional diffusion model in Equation 1.3 below to describe lateral charge diffusion through the SiO_2 layer.

$$\frac{\partial \rho(x,t)}{\partial t} = D\frac{\partial^2 \rho(x,t)}{\partial x^2}, \tag{1.3}$$

Here ρ is the charge density and D is the diffusion coefficient. From this model, they are able to describe the relationship between lateral injection spot size (L) and the diffusion coefficient as $L^2 \propto Dt$. Using this proportionality, they can extract the diffusion coefficient as follows. First they take measurements of the full width of each injection spot at half the maximum CPD value for each KPFM image, as seen in Figure 1.5(a). To obtain the diffusion coefficient, they plot the square of the FWHM lateral spot sizes against time in Figure 1.5(b), which should form a straight line. By the proportionality presented above, the slope of this line should be the diffusion coefficient.

Our final paper calculates a diffusion coefficient and trap activation energy for the HfO_2 layer of a sample. Zhang (2016) presents a slightly different method for diffusion coefficient extraction than the simple proportionality used in Dunaevskiy and Knorr models. First, charge diffusion is described by the differential equation

$$\frac{\partial C(x,t)}{\partial t} = D\frac{\partial^2 C(x,t)}{\partial x^2} - \frac{C(x,t)}{\tau(t)}.$$

Here, the function $C(x,t)$ is the surface density of trapped charges at the injection spot and the function $\tau(t)$ is the time-dependent lifetime of the charge. While this model is still describing a physically lateral system like that in Equation 1.3, it includes a term to account for charge leaving the system, $-\frac{C(x,t)}{\tau(t)}$, where $\tau(t)$ is the time-dependent lifetime of

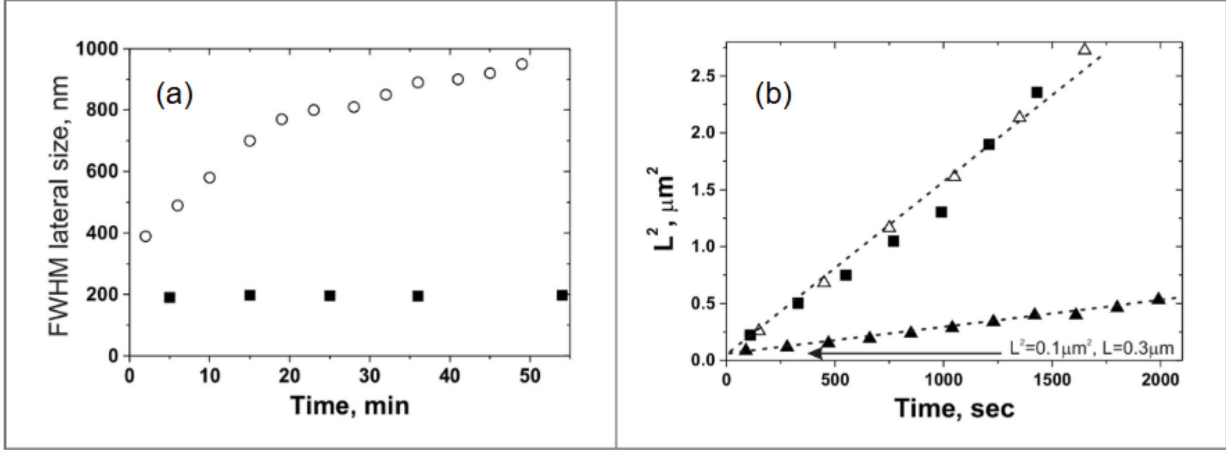

Figure 1.5: a. Lateral size (full width at the half-maximum value) of an injection spot in ambient conditions (squares) and in vacuum (circles) over time. We can see that the lateral spreading of the injection site is greatly increased in vacuum compared to ambient conditions. b. Lateral size squared over time for injection in SiO_2 (full squares) and Si_3N_4 (full and open triangles represent two different experimental runs).

the charge in the dielectric. They define $\tau(t)$ as:

$$\tau(t) = \Delta t \ln \frac{C_{tot}(t + \Delta t)}{C_{tot}(t)}.$$

Using their calculations for C_{tot}, which come from the CPD measurements recorded by KPFM images, they were able to use the Crank-Nicolson method to solve the diffusion equation and find the diffusion coefficient D.

Zhang (2016) also presented a method for extracting trap activation energy from charge diffusion KPFM measurements. They injected charge using an AFM probe biased with − 13V on a sample with an 8-nm HfO_2 layer on top of an 8-nm SiO_2 layer. They performed a series of charge diffusion experiments at temperatures ranging from room temperature to 90°C and extracted a diffusion coefficient for each using the method outlined above. They used the equation below,

$$D = D_0 e^{\frac{-E_a}{k_b T}} \tag{1.4}$$

where D is the diffusion coefficient, D_0 is a constant, E_a is the trap activation energy, k_b is the Boltzmann constant, and T is the absolute temperature, to describe the relationship between the diffusion coefficient and absolute temperature. Using a series of diffusion coefficients for the HfO_2 at different temperatures, they were able to calculate trap activation energy, as seen in Figure 1.6.

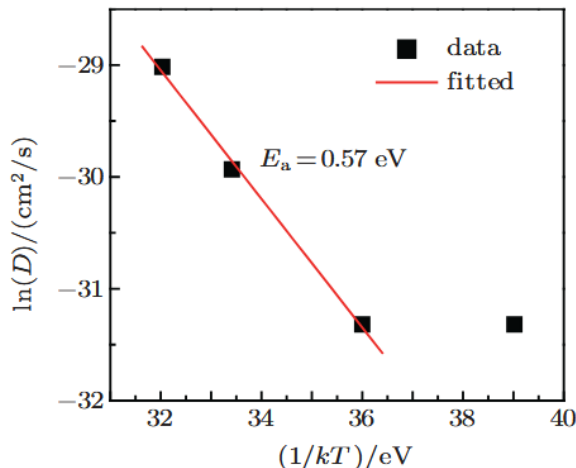

Figure 1.6: Natural log of the diffusion coefficient plotted against $\frac{1}{k_b T}$. The slope of this line is the trap activation energy[5]

The trap activation energy can yield useful information about dielectric defects and oxide-semiconductor integration quality.

1.5 Summary and Outline of the Thesis

Now that we have introduced the background motivation and physics involved in this thesis, we can discuss the ultimate goal of this project. We are working with Rafael Jaramillo and Rishabh Kothari, collaborators who have expertise in materials synthesis and properties, and aim to demonstrate the functionalities of these materials for applications in microelectronics. They collaborators are working on methods to integrate high-k dielectrics with 2D TMDs for applications in novel transistor technology. In the Aidala Lab, we are characterizing the integration quality of samples provided by our collaborators using local defect characteri-

zation techniques. This work will eventually be used to provide feedback on the quality of different integration techniques employed by our collaborators. As we are in the early stages of this project, we are mostly working on characterization technique development–the work presented in this thesis. We've been working with a HfO_2/MoS_2 sample, where HfO_2 is the dielectric, and MoS_2 is the 2D TMD. In Chapter 2 we will present our technique in detail, and in Chapter 3 we will present the process involved in developing that technique, along with our best results. Chapter 4 will discuss the future directions of this project and how our results connect to the prior work presented in Section 1.4.

Chapter 2

Methods

The work in this thesis seeks to investigate the interface between HfO_2 and MoS_2 through dielectric characterization of the HfO_2 layer with charge diffusion measurements on an atomic force microscope. In this chapter, we will outline the procedure used to make these measurements, including sample fabrication, atomic force microscopy (AFM), environmental controls, charge injection, and diffusion monitoring. The bulk of the experimental work done for this thesis went towards developing the procedure outlined in this section. The details behind its development are described in Chapter 3. We will begin our discussion of the experimental procedure with sample fabrication.

2.1 Sample Fabrication

To characterize the interface between HfO_2 and MoS_2, we will be comparing the dielectric performance of HfO_2 deposited on MoS_2 against its performance when deposited on silicon, as HfO_2/Si is a well-studied dielectric/semiconductor system. To make this comparison, our sample has regions of HfO_2 deposited on MoS_2 and silicon in close proximity.

Sample fabrication is performed by our collaborators at MIT, graduate student Rishabh Kothari working in the lab of Rafael Jaramillo. The process begins with a solvent-cleaned silicon wafer. While this wafer is in principle "bare", it has a thin native SiO_2 oxide layer on

its surface. MoS_2 is sourced in a crystal form from HQ Graphene. It comes in discrete multi-layer flakes varying in lateral size from 1 μm to 50 μm. These MoS_2 flakes are transferred to the silicon wafer using lab-grade tape in an exfoliation process as follows. The tape is pressed over top the MoS_2 flakes and pulled upward. The tape with MoS_2 flakes is then pressed on top of the silicon wafer. The flakes adhere to the silicon wafer and the tape is pulled away, taking the top few layers of each MoS_2 flake with it. This leaves a flat, pristine layer on top of each flake.

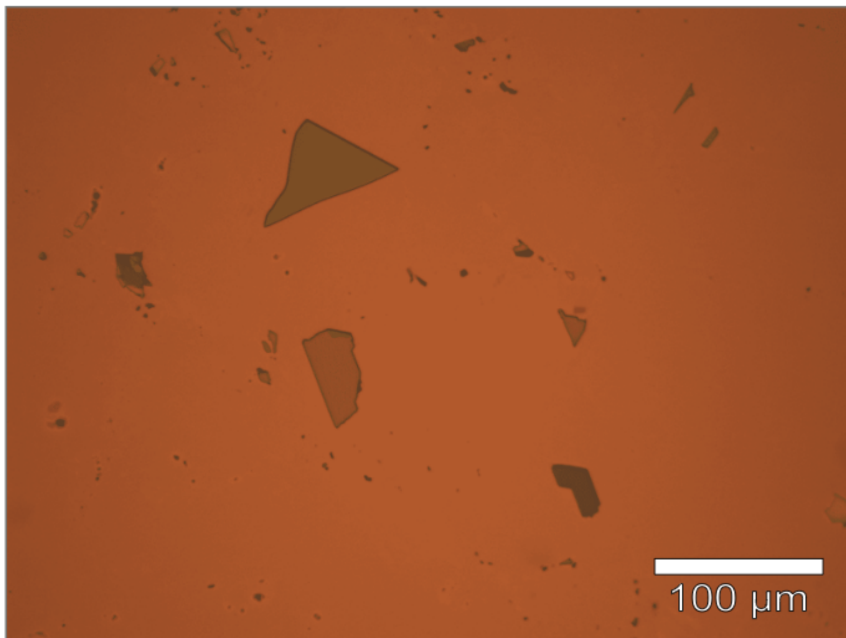

Figure 2.1: Optical microscope image of the sample after MoS_2 flakes have been exfoliated on the silicon wafer, prior to HfO_2 deposition. The silicon wafer shows up orange in the image, and the flakes are varying shades of brown.

As we can see in the optical image in Figure 2.1, the MoS_2 flakes show up in varying shades of brown due to the range of flake height that results from the growth and exfoliation process. When the MoS_2 is exfoliated onto the silicon, varying numbers of layers are transferred from the exfoliating tape to the surface, leading to height variation. In our topographic study of the sample, flakes were found to have heights ranging from 5 nm to 250 nm.

After MoS_2 exfoliation, HfO_2 is deposited over the entire sample using plasma-enhanced atomic layer deposition (PE-ALD). In ALD, the surface of the deposition substrate is exposed

to gaseous chemical precursors which react to form conformal monolayers. Thermal activation is typically used to induce reactions between the precursors and the substrate. PE-ALD uses plasma gases (a mix of neutral and charged particles) to induce the reactions that form the monolayers, meaning less thermal energy is needed for the deposition process [37]. Our PE-ALD process is as follows: a pulse of the precursor Tetrakis(dimethylamido)hafnium, a N_2 purge, an exposure of plasma O_2, followed by another N_2 purge. This cycle is repeated 80 times to form a uniform layer of HfO_2 over the entire sample that is about 10 nm in height. It is worth noting that in contrast to commercial high-quality films, our HfO_2 deposition is not done on a pristine surface. There is no cleaning step between MoS_2 flake deposition (which leaves a tape residue on the silicon substrate) and the HfO_2 PE-ALD deposition. The possible consequences of this lack of cleaning step are discussed further in Chapter 4.

2.2 Atomic Force Microscopy

Fundamentally, atomic force microscopy (AFM) uses a physical probe with a radius on the scale of tens of nanometers to investigate the topographic, electrical, magnetic, and ferroelectric properties of materials. All our sample characterization measurements were taken on an MFP-3D Infinity Atomic Force Microscope, manufactured by Oxford Instruments.

2.2.1 Basic Principles

The simplest form of AFM imaging, Contact Mode, drags an AFM tip along the sample to extract topographic information about its surface. We did not use Contact Mode for topographic imaging in this project, as this form of imaging can cause unnecessary damage to the sample surface and tip. We instead used AC Tapping Mode to do topographic characterization. A diagram of the basic AFM setup is shown in Figure 2.2(a).

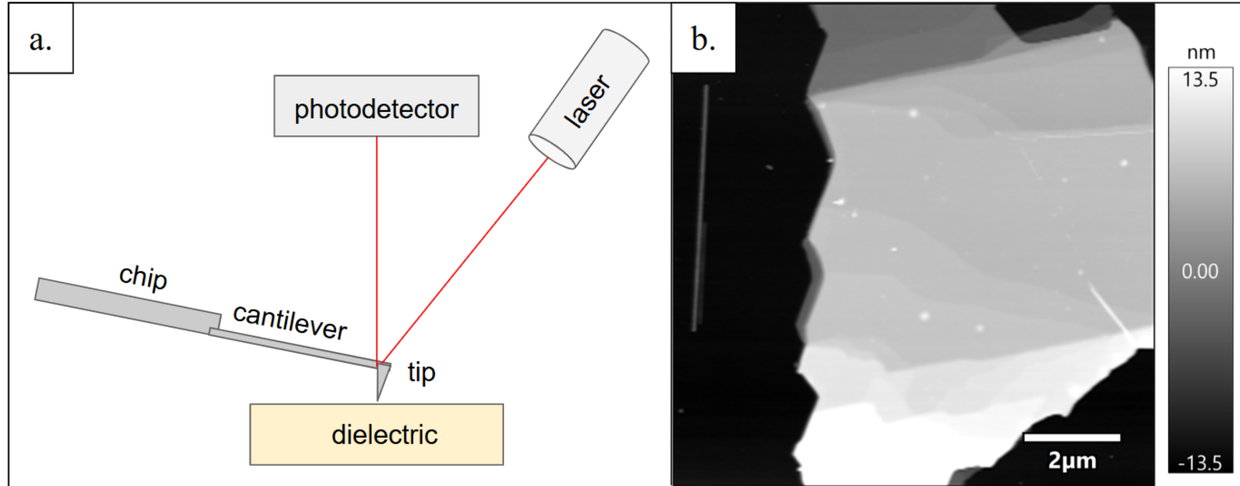

Figure 2.2: a. Basic AFM AC Tapping Mode setup. Relevant setup components are labeled. b. AC Tapping Mode image of our sample, showing one MoS_2 flake over the silicon substrate. The brighter sections of the image are the flake. The tallest region of the flake is at the bottom of the image, and each darker plateau on the flake signifies a region with fewer MoS_2 monolayers.

The AFM tip, which is used to interact with the sample, actually has three components: a main chip, a cantilever that is free to oscillate, and a tip apex that protrudes off the end of the cantilever. It is this final piece of the tip that actually makes contact with the surface.

In AC Tapping Mode, the cantilever is driven to oscillate in air using a piezoelectric stack which expands and contracts in response to an applied oscillating voltage. By scanning the oscillating tip over the surface of the sample, topography can still be tracked as in Contact Mode, simply with less damage to tip and sample due to the reduced contact time between the two. The motion of the tip is recorded by reflecting a laser off the back of the cantilever onto a photodetector. An example topographic image is shown in Figure 2.2(b).

For AC Tapping Mode, the tip is driven to oscillate at a set amplitude where the tip just encounters the surface at the bottom of each downswing. As the tip is scanned over the surface of a sample, any contours or raised features the tip encounters will alter the amplitude of the tip. In response to amplitude changes, the tip will move up or down to regain the set amplitude, thereby tracking the surface topography of a sample.

2.2.2 Kelvin Probe Force Microscopy

The work in this thesis makes use of electrical measurements obtained using the Kelvin Probe Force Microscopy (KPFM) mode. KPFM is a dual-pass technique, meaning for each line of the scan, the tip scans over the sample section twice. For KPFM, the first pass is an AC Tapping pass to record sample topography, and the second pass is a KPFM measurement which records the potential difference between the sample and the tip. The dual-pass technique allows for correlation between the sample topography and KPFM measurements.

During the KPFM pass, the tip is raised a set height above the surface of the sample, and an AC voltage is then applied to the tip. A simple schematic of the KPFM setup is shown in Figure 2.3.

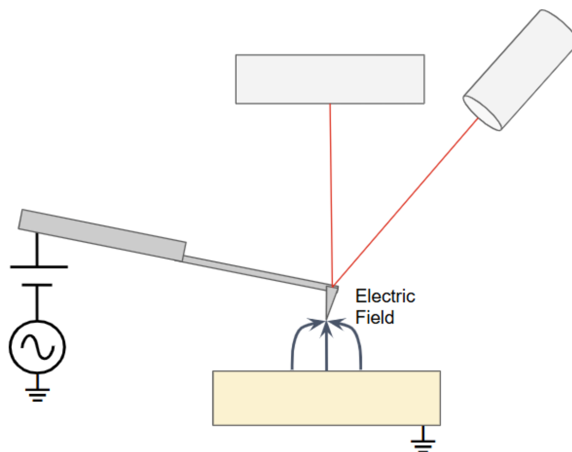

Figure 2.3: AFM KPFM setup. All physical components are the same as those in the diagram for AC Tapping Mode.

There is always a DC electric field present between the tip and sample. The potential associated with this electric field is V_{CPD}, the contact potential difference between tip and sample. When the AC voltage ($V_{AC} = A\sin(\omega t)$) is applied to the tip, it causes the tip to experience attractive and repulsive forces, making it oscillate. The magnitude of these oscillations changes based on the magnitude of V_{CPD}, and V_{CPD} changes based on the electrical properties of the sample. At each point in the KPFM image, a feedback loop applies a DC offset voltage to the tip to nullify the tip oscillations. The magnitude of this

offset voltage is equal to the magnitude of V_{CPD}. The V_{CPD} between tip and sample can change for a few reasons, including trapped charges in the sample, which is what we are interested in for this experiment. The DC offset required to neutralize the physical tip oscillations is recorded and converted into a map of the surface potential. The topography and potential images from a KPFM scan are shown in Figure 2.4.

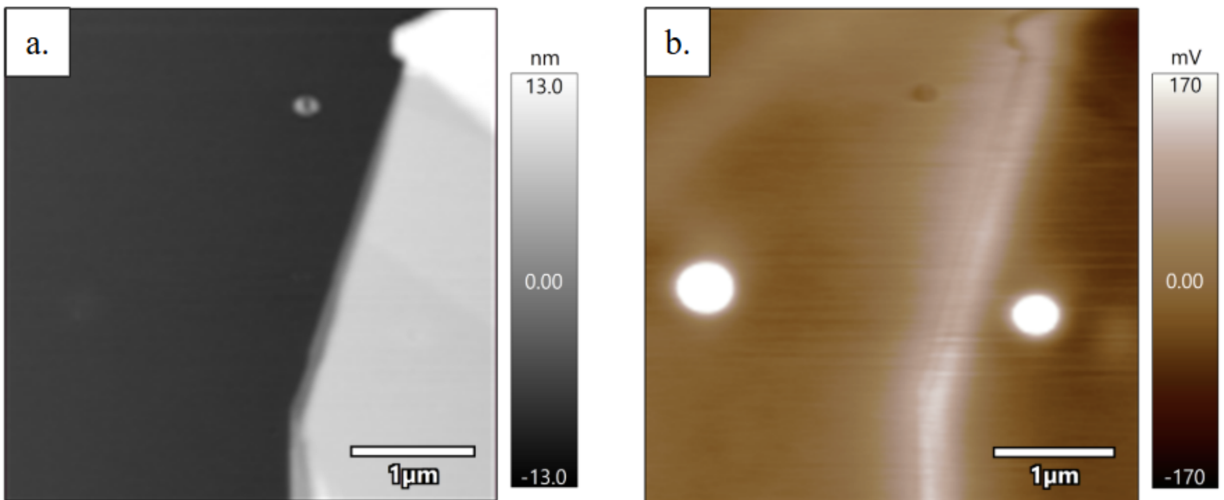

Figure 2.4: a. Topographic image produced during a KPFM scan of our sample. b. Surface potential image produced during a KPFM scan of our sample. We can see how topography aligns with the potential measurements: the bright line through the middle of the image is the edge of a flake on the sample surface.

We can see an MoS_2 flake (light gray) and silicon substrate (dark gray) in Figure 2.4(a). Charge diffusion spots produced by the injection procedure described in Section 2.3.3 show up as bright white circles in Figure 2.4(b). The edge of the MoS_2 flake can also be seen in the potential image of Figure 2.4. This may be due partially to coupling between topography and potential measurements for the given KPFM scan, but it may also be due to a difference in potential between tip and surface on and off the flake.

2.3 Charge Diffusion Measurements

In this section, we present an overview of the procedure for charge diffusion measurements, along with the rationale for certain steps. The full, detailed procedure is provided in Appendix 1.

2.3.1 Sample Holder

Our sample is set up for AFM measurements in a specialized sample holder that performs three functions. First, it grounds the sample for electrical measurements, ensuring that no stray charges or current are able to damage the sample or electronics. This connection also provides a ground reference for our potential measurements. Second, it is able to heat the sample. We perform charge injection and charge diffusion measurements at elevated temperatures. Third, it has an opening through which nitrogen can flow. Figure 2.5 shows our sample in its holder for AFM.

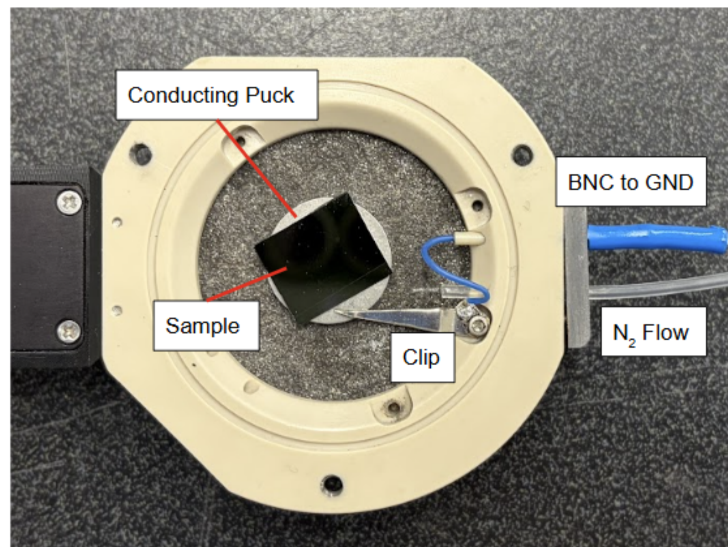

Figure 2.5: Picture of the sample mounted on its sample holder. The BNC connection to ground and plastic tube for nitrogen are labeled. The grounding BNC is connected through a wire and conducting clip to a metal puck.

The sample is mounted on a conducting puck using silver paint in order to ensure an

electrical connection between the two. A metal clip connects the conducting puck to a grounding BNC cable and also holds the sample/puck in place. An insulating mica disk is placed between the conducting puck and the sample holder itself to protect the sample holder from currents generated during AFM measurements.

2.3.2 Environmental Controls

Our sample is left in ambient conditions between experimental runs, meaning a water layer forms on its surface. This water layer can have a large impact on the results of charge diffusion experiments, as is reported in Wang *et al.* and Dunaevskiy *et al.* [32][35]. We make several efforts to get rid of this water layer and image in a dry environment.

The AFM tip is mounted into a holder with a flexible black membrane attached. When the tip holder and sample holder are in place for AFM measurements, a loose seal is formed by the black membrane with the sample holder, enclosing the tip-sample system. The tip holder and tip-sample system are pictured in Figure 2.6.

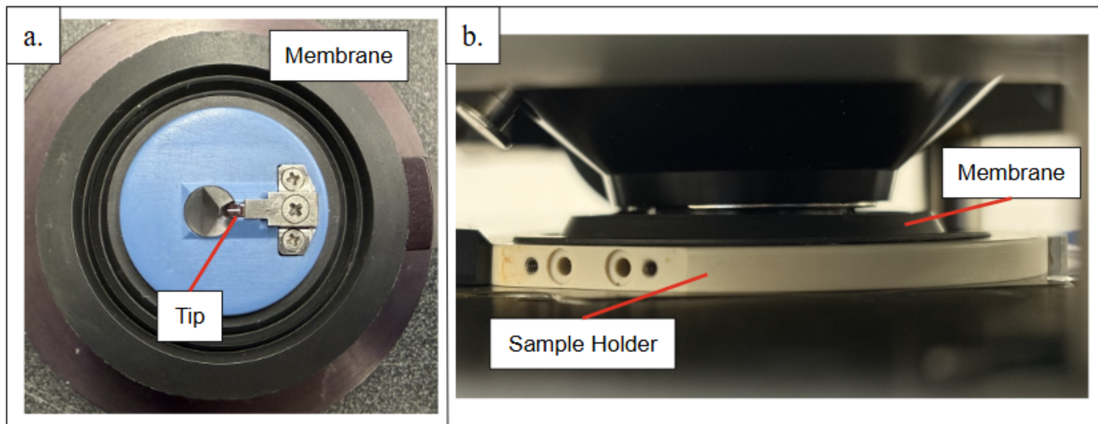

Figure 2.6: a. Tip holder with the flexible black membrane attached. A tip is mounted on the tip holder. b. Tip holder and sample holder in place for an AFM measurement. The tip holder is held blue side-down over the sample holder, creating a loose seal of the tip-sample system.

The night before a charge diffusion experiment, the tip and sample are set up for imaging. We complete a series of performance checks on the tip (topographic imaging, KPFM imaging,

and charge injection) and then begin flowing nitrogen into the tip-sample system. We maintain a flow rate such that the lighter float indicator is at 110±5 mm and the heavier float indicator is at 45±5 mm. We rely on positive pressure in our tip-sample setup to create a dry nitrogen environment because we only have a loose seal around the system. As nitrogen gas is continuously pushed into the tip-sample system, it should force out the already-present air and prevent other air molecules from entering. We leave this set up for at least 10 hours before beginning charge diffusion measurements.

After the extended nitrogen exposure, the sample is heated in order to evaporate lingering water molecules. We slightly raise the tip off the surface before heating the sample to 150°C and holding there for 15 minutes. The tip is raised off the surface by five turns of the front leg of the head to account for thermal expansion and shifting in the sample. When the tip remains in contact with, or simply close to, the surface during the heating process, thermal drift of the tip and surface features can cause the tip to bend and twist, causing permanent damage.

2.3.3 Charge Injection

After the sample is heated to 150°C, it is cooled down to 70°C for charge injection. The sample is left for five minutes after reaching the desired temperature to equilibrate. After the equilibration period, the tip is retuned and reengaged with the surface to account for any tip and/or surface changes that occurred due to the temperature fluctuations. Charge is injected at 70°C because it yields larger amounts of trapped charge than when the injection is performed at room temperature, as reported in Zhang (2016)[5].

We inject charge in the HfO_2 layer over both MoS_2 flakes and the silicon substrate. Locations for injection are chosen at the edge of a flake so that the two resulting injection spots can be easily captured in one KPFM image with high resolution, generally within a 10 μm square. The MoS_2 flakes used for injection and subsequent charge diffusion measurements are selected for large, flat surface layers. Such flake surfaces are generally found on MoS_2

flakes that are 20 nm in height and shorter.

To perform the injection, the tip is brought into contact with the surface in Contact Mode. In this case, Contact Mode is not used as a scanning technique but as the software setup that allows for point contact with the surface. For injection, the tip is lowered to the surface. Once the tip makes contact, it is held in place while a voltage is ramped in the tip. We use a 0.1 s ramp to bring the tip voltage from 0 V to 4 V. The tip is then held at 4 V for two minutes, after which the tip voltage is ramped back down to 0 V over 0.1 s. All injections and KPFM measurements are taken using an Adama AD-42-AS conducting diamond probe. When injecting charge, we do not want to damage the dielectric, and so we monitor the current passing from tip to sample. This is done by connecting the clip attached to the mounting puck to a current preamplifier with a sensitivity of 1 $\mu A/V$.

2.3.4 Diffusion Measurements

Following charge injection, we can begin charge diffusion monitoring. We perform the diffusion monitoring at 90°C. After bringing the sample to this temperature, we allow a five minute equilibration period, followed by retuning and re-engagement with the surface. Diffusion measurements can be performed at room temperature or elevated temperatures–in fact comparisons of diffusion experiments at a range of temperatures can yield trap activation energy for the dielectric under study. We chose 90°C because it speeds up the diffusion process as compared to room temperature, allowing for faster collection of diffusion data. The 90°C temperature was suggested by Zhang (2016)[5]. Charge diffusion is monitored by continuous KPFM scans over the region where charge was injected. Diffusion is monitored for at least six hours. Periodically throughout this scanning process, the tip is retuned and reengaged with the surface to account for any changes in the tip-surface system or drift in the tip height that occurs over the course of imaging.

Our KPFM images are 256 x 256 pixel images, acquired line by line in the horizontal direction. Each pixel is one measurement of the potential difference between tip and sample.

To extract the potential data used for diffusion analysis, we take the potential measurements from line slices over our charge diffusion spots. We use 100 nm wide line slices that are laid horizontally through the maximum CPD value over each charge injection spot. Every data point of these line slices averages the potential value in the 50 nm directly above and directly below it. A figure of this process can be seen below in Figure 2.7.

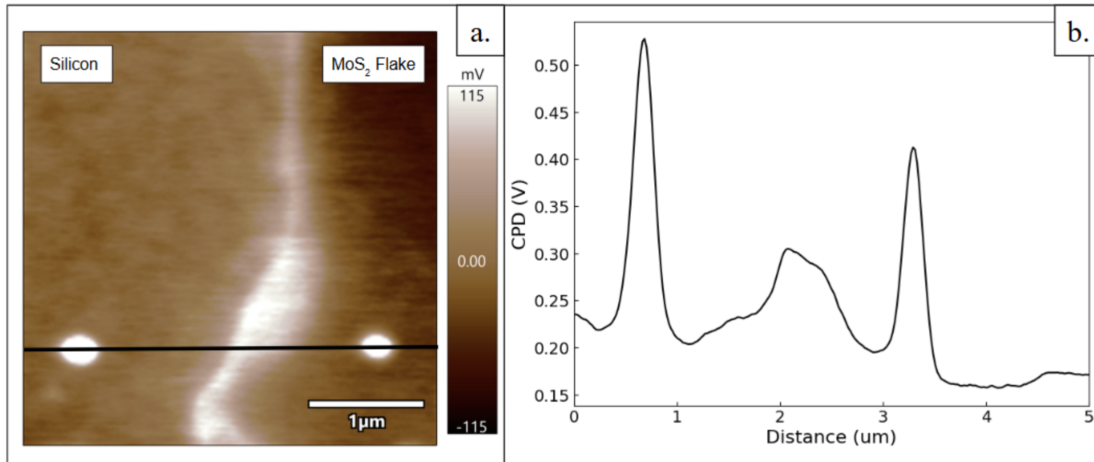

Figure 2.7: a. Example KPFM potential image with a line slice drawn through it. b. Plot of the line slice. The horizontal slice averages over 100 nm.

By extracting a value of maximum CPD from each line slice, the change in potential, and therefore diffusion behavior, over time can be tracked. The CPD value for each image is extracted by recording the difference between the maximum CPD value in the charge injection spots and the background potential value.

Chapter 3

Results and Analysis

In this section we will present the results of charge diffusion experiments performed on our $HfO_2/MoS_2/Si$ sample using KPFM. The majority of the work in this thesis served to develop a reliable procedure to compare charge diffusion in dielectrics on different substrates. To that end, we present a series of experiments used to develop our experimental procedure. Our early experiments were primarily performed on an HfO_2/Si sample to refine injection parameters. We also present the development of our environmental controls through a series of experiments in varied environmental conditions, including ambient conditions, nitrogen, and nitrogen with sample heating. Charge diffusion behavior is visualized using both KPFM images and plots of maximum potential values over time. Lastly, we discuss preliminary analysis of the charge diffusion behavior, which yields calculations for charge density and the decay time constant of diffusion resulting from curve fitting of our CPD data.

3.1 Initial Experiments: The Importance of Environmental Control

We begin with three charge diffusion experiments, each performed under different environmental conditions. The first is done in ambient conditions, the second in dry nitrogen, and

the third in dry nitrogen with pre-injection heating of the sample. Each successive layer of environmental alteration was an effort to control the water layer that forms on oxides left in ambient conditions, and understand if there was a measurable difference in charge diffusion behavior when the effects of the water layer were mitigated.

3.1.1 Ambient Conditions

While ultimately our experiments were conducted in controlled environmental conditions, we started with charge diffusion experiments in ambient conditions to begin developing an experimental procedure. The goal of this charge diffusion experiment was to determine the parameters we would use for charge injection. Injection was performed on a sample that consisted only of a silicon wafer with 80 cycles of PE-ALD HfO_2 deposited on top, yielding a 10 nm oxide layer.

A grid of injection locations was created on the sample surface with injection voltages of ±3V, ±4V, and ±5V. Each voltage was used for three different injection spots, one held for 10s, one for 30s, and one for 60s. We can see in Figure 3.1 that over the course of one hour of KPFM monitoring for charge diffusion after injection, the magnitude of the contact potential difference (CPD) between tip and sample decreased.

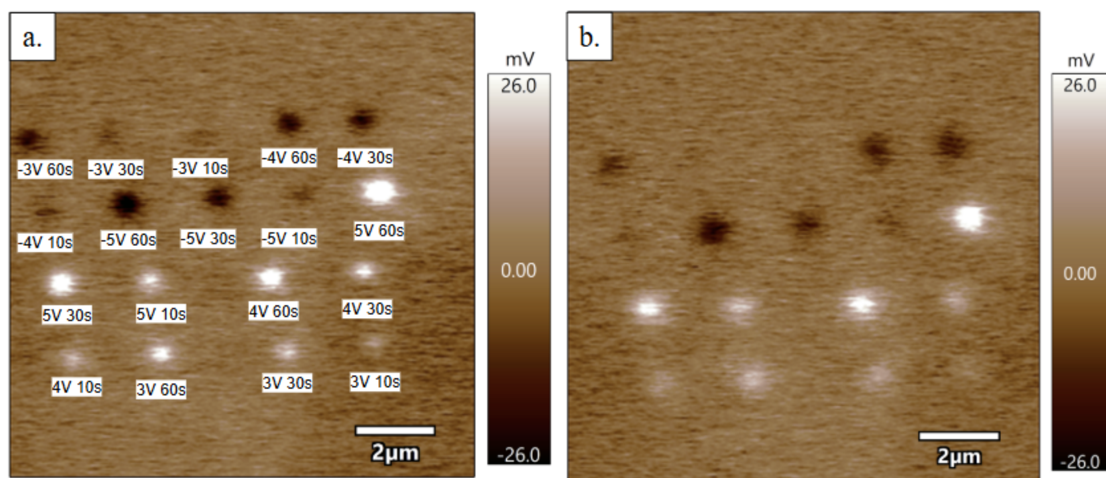

Figure 3.1: a. A grid of injection points 33 minutes after injection. in ambient conditions. b. The grid of injection points 61 minutes after injection.

The CPD measured between tip and sample is a result of charges in the sample that were trapped during the injection process. Thus, when the CPD decreases, it is measuring the effects of charge diffusing through the HfO_2 layer. This charge diffusion experiment was the first attempt at injecting charge and measuring its diffusion using KPFM. The CPD values measured in this experiment are not typical of those measured in later experiments, but the results are worth reporting to demonstrate the effect of hold time and injection bias on the resulting CPD between tip and sample.

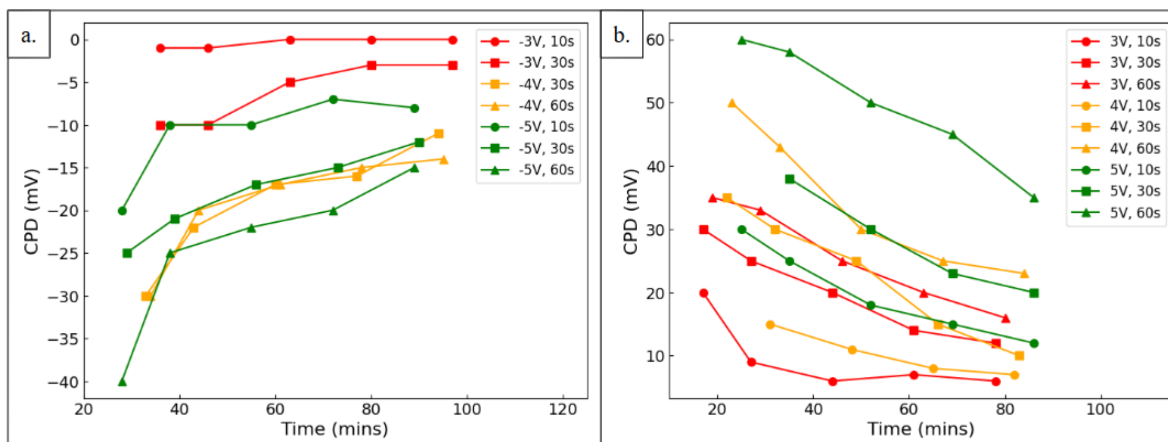

Figure 3.2: CPD over time in ambient conditions for different injection parameters. The measurements for -3V, 60s and -4V, 10s are missing due to poor positioning of the scan window missing the injection locations for multiple KPFM runs resulting in only two data points for each.

As we can see in Figure 3.2, a larger absolute injection voltage and longer hold time generally results in a higher absolute CPD after injection. This same behavior can be seen in Figure 3.1 – injection spots for the longest hold times are brighter (for positive injection) and darker (for negative injection) than the surrounding spots for the longest hold times. The observed correlation between injection voltage and hold time was used to inform the injection parameter selection for later charge diffusion experiments with environmental controls. After these initially promising results in ambient, we needed to replicate them in a dry nitrogen environment. We expected to record different behavior in a dry nitrogen environment given previous reports that the water layer can provide a path for charge to

leave the sample[32][35]. If we observed the same behavior, we would be able to continue experiments in ambient.

3.1.2 In Nitrogen

We performed charge injection and charge diffusion monitoring in a dry nitrogen environment as a first attempt to remove the water layer. Following the nitrogen procedure outlined in Section 2.3.2, we set up our tip-sample system in an over-pressured environment that had nitrogen constantly flowing in for 10 hours before beginning the experiment. We ran a charge diffusion experiment on the HfO_2/Si sample in this nitrogen set up to understand how diffusion in nitrogen, which ostensibly reduced the water layer present on the surface of our sample, compared to charge diffusion in ambient conditions in which a water layer is certainly present. Voltages of $\pm$5V and $\pm$6V were used. Hold times of 7 seconds were used for the $\pm$6V injections, while hold times of 5s and 10s seconds were used for the $\pm$5V injections. A KPFM scan taken immediately after injection is shown in Figure 3.3

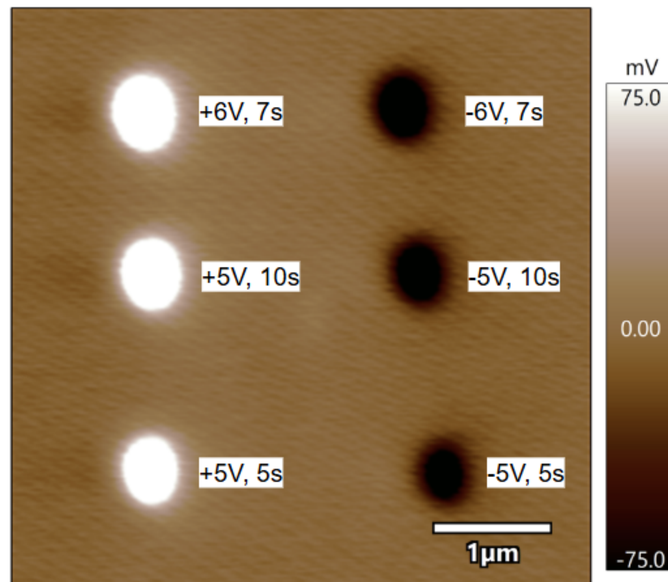

Figure 3.3: Potential image taken during KPFM monitoring of the charge diffusion experiment in a dry nitrogen environment with no sample heating. The injection parameters for each charge injection spot is labeled.

The magnitude of the CPD measured immediately following injection was over 100mV for each of the injection spots. This CPD is comparable with CPD values reported in similar experiments in the literature [5][4][30]. We can see the reduction in CPD magnitude over the first three hours of diffusion for these injection spots in Figure 3.4. Overall, the magnitude of the CPD decreased by 23% on average over 24 hours for all injection parameters. Given the larger CPD measurements in nitrogen compared to ambient conditions for similar injection parameters, we concluded that the nitrogen environment did have an impact on the water layer and our diffusion results.

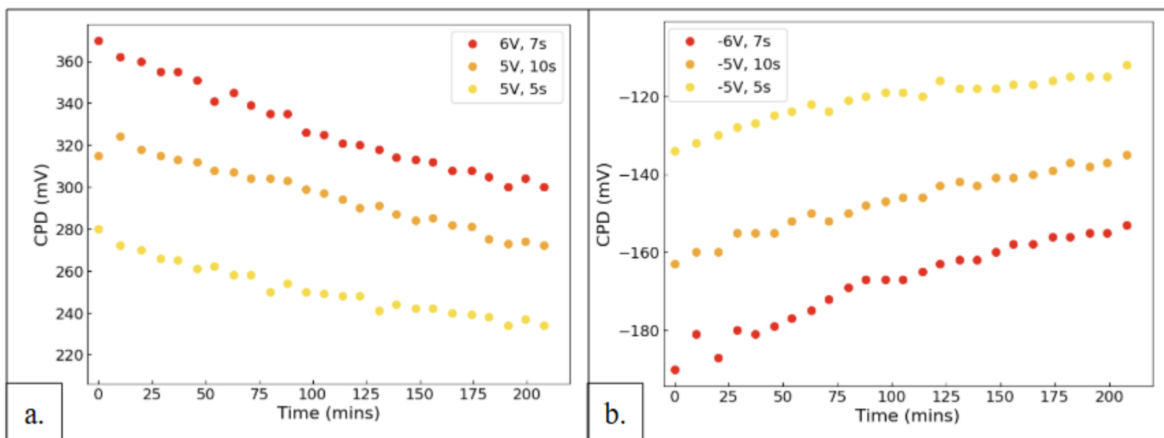

Figure 3.4: a. Maximum CPD of each injection spot with reference to the background for all positive injection voltages at select times. b. Maximum magnitude of CPD of each injection spot with reference to the background for all negative injection voltages at select times.

We can see the first three hours of charge diffusion in Figure 3.4. The magnitude of the CPD due to injections from a positive tip bias compared to injections from a negative tip bias are uniformly larger. This behavior holds across different experimental setup conditions, as seen in the previous section.

3.1.3 Pre-Injection Heating

In addition to a dry nitrogen environment, multiple papers reported heating the sample above the boiling point of water in order to drive off any remaining water layer [5][30][38]. After seeing how reduction of the water layer with nitrogen affected our results, we wanted

to take further steps to eliminate it. In this experiment, we follow the procedure outlined in Chapter 2, with the exception of heating during injection and diffusion KPFM measurements. As described in the Chapter 2 procedure, nitrogen flowed for at least 10 hours prior to heating and throughout the entire measurement process, after which the sample was heated to 150°C and held there for 15 minutes prior to injection. For this experiment where injection was performed at room temperature following heating to 150°C, the sample was left to thermally equilibrate for at least an hour prior to injection. It was at this point in the procedure development process that we moved to using the full $HfO_2/MoS_2/Si$ sample described in Section 2.1.

When keeping the injection hold times used in ambient and nitrogen-only conditions, charge injected in nitrogen with a heating step did not appear to diffuse on a time scale that was feasible for us to measure. The CPD measurements of the injected charge yielded values much less than those measured in the nitrogen-only runs. In order to increase the amount of charge injected into the HfO_2 layer, we increased the injection time to two minutes. While increasing the injection time helped with getting injection spots with enough charge to have measurably diffusive behavior, the CPD magnitude results were inconsistent. Here, we present one of the more successful runs.

Charge was injected using a tip biased to 6V and held in contact with the surface for two minutes. As mentioned above, consistent CPD results were difficult to achieve for this set of environmental controls. To compensate, we moved from injecting at multiple spots for both positive and negative biases to a single positive injection spot in both regions of interest. A KPFM image of the potential after charge injection can be seen in Figure 3.5. The potential spot formed due to charge injection on the flake (bottom left) and off the flake (top right) show some visual differences in size and brightness, indicating a larger amount of charge injected off the flake than on it. This pattern of the CPD for the injection on silicon being higher than that for the injection on MoS_2 held throughout all experiments on the $HfO_2/MoS_2/Si$ sample.

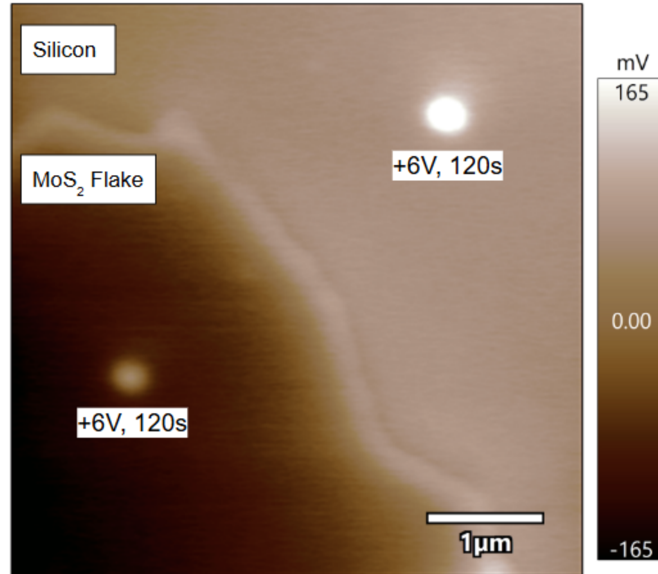

Figure 3.5: Potential image produced during KPFM scanning of the surface of the $HfO_2/MoS_2/Si$ sample following charge injection at 6V for two minutes. The sample was left in nitrogen for 10 hours and heated to 150°C for 15 minutes prior to injection.

For this experiment, the charge diffusion was monitored constantly for 12 hours using KPFM, with one final measurement being taken 12 hours after the conclusion of the continuous imaging. We present a plot displaying the maximum CPD at each injection spot over time in Figure 3.6(a).

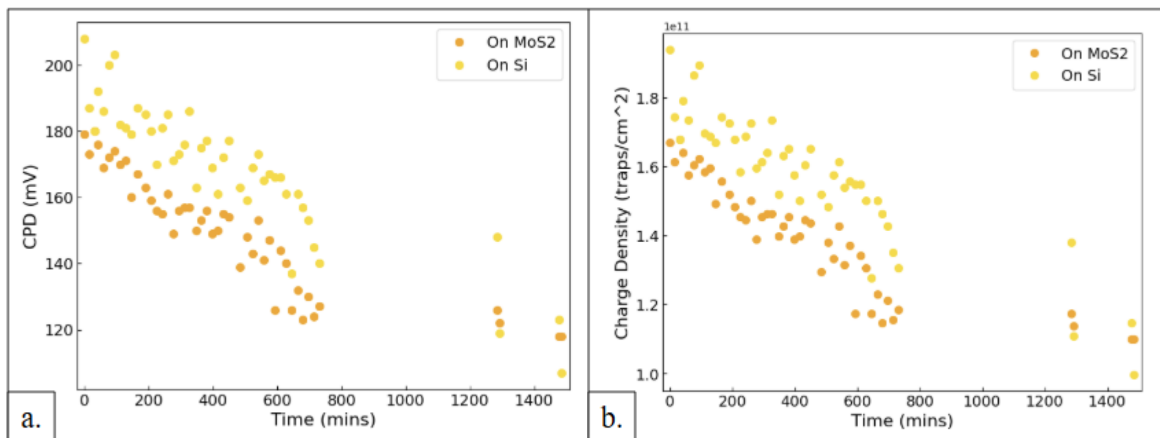

Figure 3.6: a. Maximum CPD value at each injection spot measured in reference to the background potential value over time. b. Charge density at each injection location over time.

There was an average CPD reduction of 37% over 24 hours for this charge diffusion experiment. This was a slower rate of CPD decrease than that observed in the nitrogen-only procedure. We made a charge density calculation for the injection in this pre-diffusion heating experiment using the parallel plate model outlined in Chapter 1. For a $6MV/cm^2$ bias, we found an initial charge density of $1.7x10^{11}$ traps/cm^2 on MoS_2 and $1.9x10^{11}$ traps/cm^2 on silicon The full results are displayed in Figure 3.6(b).

Across our three iterations of environmental control procedures, we observed three different CPD responses for comparable injection parameters. These differences told us that environmental control to reduce the water later has a significant impact on the results of charge diffusion measurements. Injection in ambient conditions yielded the lowest CPD values. When we moved to a dry nitrogen environment, the measured CPD values greatly increased, but the pace of diffusion slowed. Both of these changes indicated that the nitrogen environment was reducing the water layer, and that the water layer does impact charge diffusion measurements. Moving to a procedure with a dry nitrogen environment and a heating step, the magnitude of CPD measurements decreased, but the diffusion speed slowed again. This once again suggested that the effects of the water layer were being mitigated in a manner that was significant to our charge diffusion measurements.

3.2 Diffusion at Elevated Temperatures

In the previous section, results were presented for charge diffusion measurements conducted on a sample with HfO_2 deposited solely on a silicon wafer. We also presented one experiment on the $HfO_2/MoS_2/Si$ sample with an in-progress environmental control procedure. These experiments were used to determine experimental parameters that would be used in our final procedure. In this section, we present the results of experiments conducted using the procedure outlined in Chapter 2 on the $HfO_2/MoS_2/Si$ sample.

As described in Section 2.3.3, we found that injecting at an elevated temperature resulted

in more charge injected for the same injection parameters at room temperature. This was an easy fix for the challenges we experienced reliably getting enough trapped charge with injection at room temperature. At our injection temperature of 70°C, the tip bias voltage had to be lowered from 6V in the previous section to 4V. When injection was attempted with 6V at 70°C, current was measured through the dielectric, meaning a bias stress large enough to induce dielectric breakdown had been applied to the sample. The hold time remained at 2 minutes. Injection was performed in HfO_2 over an MoS_2 flake and silicon in order to facilitate the comparison of HfO_2 performance when deposited on the two different semiconductors. A potential image taken during KPFM measurements of the injection spots is shown in Figure 3.7. The KPFM measurements for this experiment were taken at 90°C.

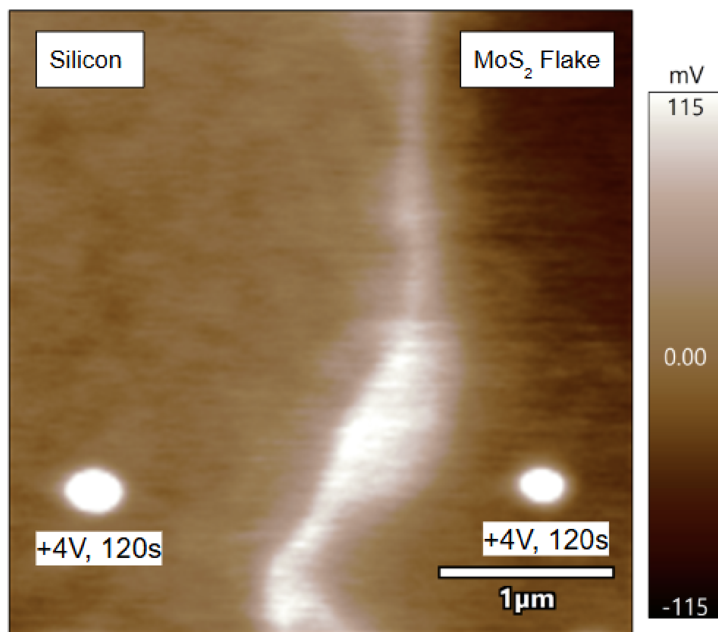

Figure 3.7: Potential image taken during KPFM scannning of the $HfO_2/MoS_2/Si$ sample following charge injection at 4V for two minutes. The sample was left in nitrogen for 10 hours and heated to 150°C for 15 minutes prior to injection. Injection was performed at 70°C, and diffusion measurements were taken at 90°C.

We extracted the maximum CPD at each injection spot with reference to the background potential for each KPFM scan over the course of the six hour measurement period. It should be noted that the maximum CPD measurements are extracted from the raw data, with no

image flattening modifications applied. Thus, the maximum CPD is calculated in reference to the local background potential, not a universal background potential for the entire sample. All of the KPFM and topography images shown in this thesis have a histogram image flattening applied, in which a histogram of each scan line is produced and used to smooth the subsequent line, so as not to distract from the relevant features in the images.

The maximum CPD data is shown below in Figure 3.8. At around the 320 minute mark, we can see that the CPD measurements on both MoS_2 and Si jump up. That was due to the tip hitting the surface during scanning. This event altered the physical relationship between the tip and sample in a manner such that all the CPD measurements across the sample were raised by approximately 45 mV.

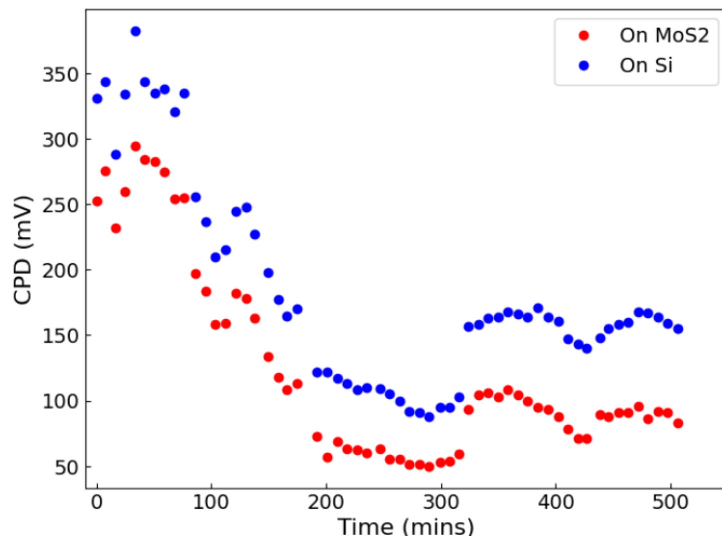

Figure 3.8: Maximum CPD over time for 4V, 2 minute injections in HfO_2 on MoS_2 and Si.

In order to complete our analysis on the charge HfO_2 diffusion behavior, we subtracted the collision-induced CPD offset from data following the tip-sample contact. While this may prevent quantitative parameter comparison for CPD measurements past the 320 minute mark, it does not significantly change the shape of the diffusion behavior. This discussion seeks to explain the CPD jump in our data, but also serves as a motivation for taking for diffusion data that both doesn't have this kind of physical anomaly and that can serve as a

point of comparison when this kind of physical interference occurs.

From our maximum CPD data we were able to calculate the charge density, using the Choudary *et al.* model of the tip and semiconductor layer as a parallel plate capacitor introduced in Section 1.4. The maximum CPD and charge density over time at each injection spot plotted in Figure 3.9.

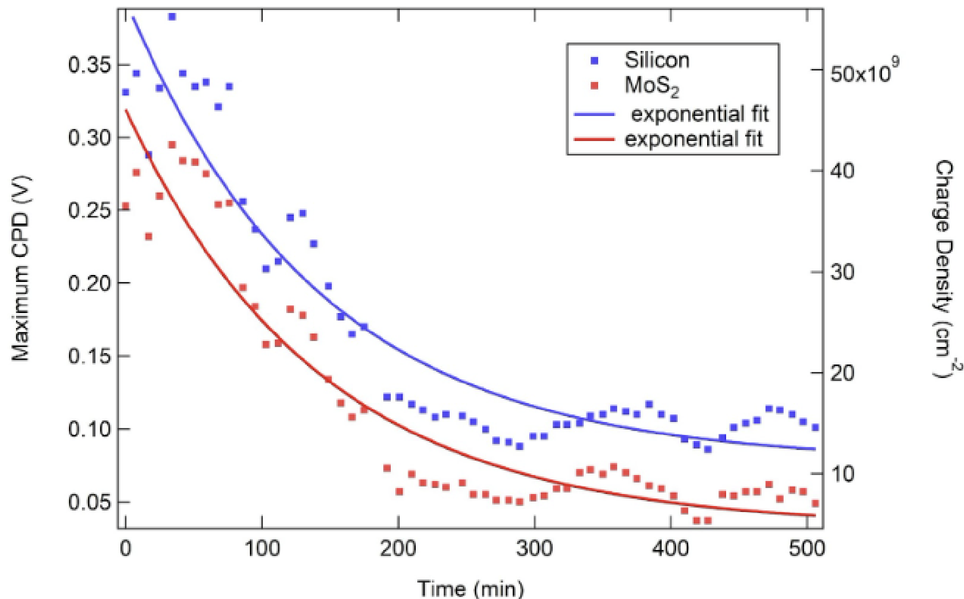

Figure 3.9: On the left axis is the maximum CPD and on the right axis is charge density. Both are plotted against time for the injection spots on and off the MoS_2 flake. Each data point can be read on both axes, on the left for its CPD value and on the right for its charge density. An exponential decay was fit to both series of CPD data.

To get an easy parameter for comparison of diffusion in HfO_2 on MoS_2 versus silicon, we fit the exponential decay function,

$$V_{CPD} = Ae^{-t/\tau},$$

to the maximum CPD data. The time constant τ is a measure of how long it takes the CPD to reduce its value by 36.8% of its original value. The time constant was found to be 142 minutes for both on the flake and off. By this first pass of comparison, there was no difference between charge diffusion in HfO_2 deposited on MoS_2 or silicon.

To understand the charge diffusion mechanism in our HfO_2, we plotted a series of CPD profiles across the injection spot on MoS_2. These cross sections, taken at a selection of times over the course of the diffusion measurements, are shown in Figure 3.10(a). These cross selections allow us to visualize the volume of the injected charge in the HfO_2 at different points in time during the diffusion process.

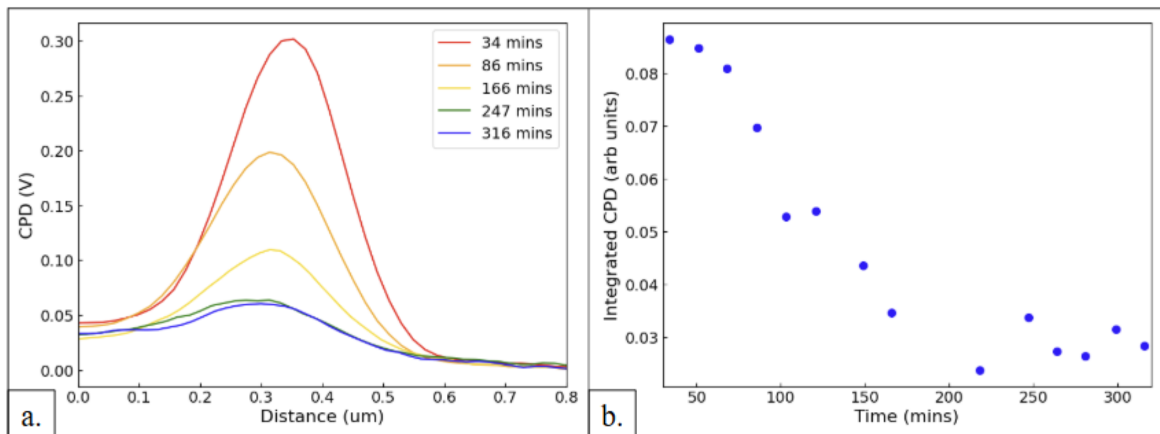

Figure 3.10: a. CPD profiles at select times during charge diffusion measurements on an MoS_2 flake. b. Integrated CPD line profiles over time during charge diffusion measurements on an MoS_2 flake.

We can see in Figure 3.10(a) that the height of the line profiles reduces over time, but the width does not increase, suggesting that the total charge in our system is decreasing. This means that charge is diffusing far enough away that it does not seem to be contributing to the potential measured between the tip and sample. Given the lack of lateral spreading in the line profiles, the charge is likely moving vertically further down into the oxide or fully into the grounded substrate, not laterally. To check our visual inspection of the line profiles, we performed a numerical integration over space of all the potential profiles in order to see if the total amount of charge was decreasing over time. The integrated CPD is plotted in Figure 3.10(b), and it does indeed decrease over time. This behavior suggests that we will need to use a vertical diffusion model rather than the lateral one that is used in the vast majority of relevant prior work for this project to describe the charge diffusion behavior. Han *et al.* report that as film thickness decreases, vertical diffusion comes to dominate over

lateral diffusion. Our film is the same thickness as their thickest film, placing it in the range for lateral diffusion, rather than vertical, which is inconsistent with our results [30].

One possible explanation for this discrepancy is that our sample was not annealed. In our review of similar experiments, samples for which lateral diffusion was recorded as the primary form of diffusion tended to have been annealed, a process in which the sample is heated to very high temperatures, reducing the number of defects in the sample. We are unable to perform annealing on our sample because of the reactivity of the sulfur in our MoS_2 layers at the elevated temperature needed for annealing.

By conducting charge diffusion experiments with different environmental setup parameters, we were able to identify satisfactory conditions under which to study charge diffusion in HfO_2, providing measurable charge diffusion within a reasonable time frame. From these experiments, we were able to extract two key characteristics describing charge diffusion behavior in HfO_2, and thus the quality of the dielectric itself: charge density and the decay time constant.

Chapter 4

Discussion and Future Work

In this work, we presented a procedure for implementing a charge diffusion characterization technique on HfO_2 using KPFM with the purpose of integrating HfO_2 and MoS_2 for next-generation transistor devices. Understanding and improving the quality of integration between high-k dielectrics and TMD semiconductors is an active area of research that seeks to develop smaller, faster, low-power next-generation transistor devices. Defect characterization of dielectrics is a key method used for studying dielectric-semiconductor integration. Local characterization techniques like Atomic Force Microscopy (AFM) combine high-resolution spatial measurements with electric measurements, providing information about material heterogeneity, and thus the nature of material defects.

We used AFM to perform a series of charge diffusion experiments with HfO_2 deposited on MoS_2 and silicon. Each successive experiment altered different parameters of the technique, such as injection tip bias, injection hold time, and environmental conditions, to develop the final procedure, which can be used to make comparisons of the characteristics of HfO_2 on two different semiconductor substrates. Through this process we were able to confirm that environmental conditions–temperature and humidity–significantly affect the results of our charge diffusion experiments. Our nitrogen and heating procedure is intended to drive off the water layer that naturally forms on any oxide left in ambient conditions. Injection

into this water layer rather than the oxide itself gives inaccurate results. Our procedure is constructed to give us the best chance at driving off the water layer without fully sealing our tip-sample system. If we come to have reason to believe that there is a remaining water layer after our environmental control procedure affecting results, we could fully enclose and seal our system in order to confirm whether there is a measurable difference.

Ultimately we hope to use this procedure to perform characterization and provide feedback on samples from our collaborators Rafael Jaramillo and Rishabh Kothari. The results from our charge diffusion work should be able to inform their growth and deposition processes in order to improve the integration of HfO_2 and MoS_2. While at this stage we are only making comparisons between HfO_2 on MoS_2 and Si on the same sample (and therefore with the same deposition procedure), in the future we would be making sample to sample comparisons to determine the best fabrication processes.

Charge diffusion measurements with KPFM have previously been used to evaluate oxide performance by calculating charge density, diffusion coefficient, and trap activation energy. Given the time constraints of this thesis, we presented only one careful experimental run measuring charge diffusion. Additional measurements are needed to perform a full statistical analysis, determine the uncertainty in our measurements, and look for variation within a sample. We also did not perform a temperature series, which has been used to extract the trap activation energy. As we plan further measurement analysis, we note that all of the parameters and parameter calculation methods reported in the literature rely on assumptions in their model of the charge diffusion system, which may not apply to ours.

Following the procedure described by Khosla *et al.* [29], we calculated an initial charge density of $3.7 \text{x} 10^{10}$ charges/cm^2 on MoS_2 and $4.8 \text{x} 10^{10}$ charges/cm^2 on silicon for an applied bias of 4MV/cm^2. In Han *et al.*, they measured an initial trap density on the order of 10^{12} with an applied bias of 13MV/cm^2 in 10 nm of HfO_2 [30]. Assuming a linear relationship between applied bias and charge density, our measured charge density is about one order of magnitude smaller than expected, using the Han charge density values. The Han group does

not report their method for calculating charge density, making it unclear whether a direct comparison between the two charge density values can be made. As for the comparison between Si and MoS_2, we noted that the charge density in HfO_2 was always higher on silicon than MoS_2, for the same injection parameters, across multiple experiments with varying environmental conditions. There are multiple possible interpretations of this result. First, it is possible that the silicon is not completely clean, which could impact the defects in the HfO_2 layer in a way unrelated to actual material integration. This is because the MoS_2 is exfoliated with tape over the entire silicon layer, leaving a tape residue over the exposed silicon substrate. The sample is not cleaned before HfO_2 deposition. Another possible explanation for this difference is that the physics of the substrates (silicon and MoS_2) impact the injection process, causing the silicon to have a higher charge density by the time we start taking measurements.

4.1 Charge Diffusion Models

One of the dielectric characteristics promised by charge diffusion experiments is the diffusion coefficient D. As discussed in Section 1.4 of Chapter 1, most of the diffusion models used in prior charge diffusion experiments assume a 2D distribution of charge either at the dielectric surface or the dielectric-semiconductor interface, and assume solely lateral diffusion, where the change in lateral size of the charge injection spot is proportional to the diffusion coefficient. We saw in Section 3.2 that we do not have any lateral spreading of our charge injection sites. Moving beyond this simple model and accurately describing the behavior of diffusing charges trapped in the HfO_2 requires careful consideration of the physical situation at hand. Dunaevskiy *et al.* [35] describes a model in which charges initially repulse each other through Columbic forces until the charges that remain are mainly deeply trapped and move through diffusion. This initial repulsion happens faster than the time is takes for us to begin our first measurement. It is not accurate to say that diffusion is the only factor at force

in this second time regime–Columbic forces still exist, though they are likely weaker than the forces driving diffusion. The actual mechanism driving the diffusion itself is another layer of complication. For solely lateral diffusion models, the simple relationship between lateral injection spot size and diffusion coefficient can give a value to characterize the diffusion. When considering models with diffusion in three dimensions, more careful consideration of the mechanisms of diffusion are required to yield a characteristic diffusion value.

The model proposed by Zhang (2016), discussed in Section 1.4, is built off the same mathematical basis as the model used in Dunaevskiy *et al.*[5][35]. In both, they make an assumption of two-dimensional (lateral) diffusion, and use a spatially-1D diffusion equation applied to slices of potential data. The Zhang model adds a term to allow for charge to leave the system, but the primary diffusion mechanism is still assumed to be lateral. A first pass at modeling our data using the Zhang method did not yield physically reasonable results. It is likely that a physical model to describe the mechanisms behind the diffusion observed in our sample will require more advanced models than those proposed in the literature we reviewed to develop our experimental process. For example, Shockley-Read-Hall statistics and Poole-Frenkel emission can be used to describe the charge carrier transportation methods in dielectrics, semiconductors, and at the interface between the two[39][40]. In such a model, extracting a single diffusion constant is not a meaningful characterization. Instead, we would consider detrapping and trapping rates that lead to charges moving through the dielectric film into the substrate.

We did not measure any significant differences in the electrical characteristics of 10 nm of HfO_2 deposited on MoS_2 versus silicon. Injection with the same parameters consistently yielded a higher CPD and charge density measurement on silicon compared to MoS_2, but there were no measured differences in the diffusion behavior of that charge in the oxide. Both sets of diffusion measurements yielded a time constant of 142 minutes. It is quite possible that any differences in electrical characteristics caused by the different semiconductor substrates are negated by the relatively thick 10 nm of HfO_2.

4.2 Future Work

Now that we have a working procedure for charge diffusion measurements, there are many steps we can take to continue the work on this project. Ideally, we would next perform repeat diffusion experiments with more injection locations, collecting enough data to perform a robust statistical analysis comparing diffusion on MoS_2 versus Si. This would give us information about sample variability, in terms of sample heterogeneity and our actual measurement uncertainty. At present, our data extraction method is manual, meaning someone must go through each KPFM image and manually take data line slices at each injection point. As we take more data, it would be beneficial to automate this extraction process to speed up the data collection and analysis process. Once the amount of data being collected is large enough, automation to extract the CPD values will be necessary.

As we develop our physical model to describe the mechanics of charge diffusion through hafnia, we can extract some parameters of dielectric quality that are agnostic to the physical model we choose. For example, the time constant that we extracted by fitting our diffusion data with an exponential decay characterizes the diffusion in a way that can be compared from experiment to experiment, but does not require a further physical model. In developing our physical model, we will need to perform another literature search for work that seeks to understand charge dynamics in materials more broadly, and understand how those models are relevant to our system.

We also hope to take a temperature series of diffusion experiments. Any physical model we choose will have temperature dependencies, with specific relationships that differ with the details of each. Model-agnostic parameters like the time constant will change with temperature, giving us a way to make temperature comparisons before landing on a description of what is happening physically. As discussed in Chapter 1, by measuring charge diffusion at a range of different temperatures, we can extract the trap activation energy of traps in our oxide. This is done using the equation,

$$D = D_0 e^{\frac{-E_a}{k_b T}} \tag{4.1}$$

where D is the diffusion coefficient, D_0 is a constant, E_a is the trap activation energy, k_b is the Boltzmann constant, and T is the absolute temperature. This calculation does give us a reason to make a calculation of a diffusion coefficient so we can use this relationship. Finding the trap activation energy would give us useful information about the trap defects in our HfO_2 oxide layer.

Ultimately, with the experimental procedure developed over the course of this thesis work, we will be able to take more charge diffusion measurements in hafnia on our current sample and future samples. We initially plan on collecting enough data to make effective comparisons of HfO_2 integration with MoS_2 and silicon on the same sample. The comparison between these two different systems will give us information about the quality of HfO_2 integration with MoS_2 where HfO_2 and Si serve as a point of comparison. We then hope to use the knowledge gained in these comparisons to move into comparing HfO_2 integration with MoS_2 on different samples with different HfO_2 deposition techniques. Making these comparisons will allow us to address the motivating scientific question of this work: how to best integrate dielectrics with 2D TMD semiconductors for novel transistor technology.

Appendix A

Charge Diffusion Procedure

A.1 The Night Before Imaging

A.1.1 Sample Setup

1. Load a conductive tip into the tip holder with a floppy black membrane
   (a) The Adama AD-40-SS tips work consistently for this setup
   (b) As of 3/28/26, AD-42-AS #4 has been working well
2. Load the sample into the heater stage
3. Move the clip in the sample holder onto the metal puck and screw it in place
   (a) NOTE: be gentle with the clip's screw! It has already had to be moved once in the holder due to stripping of the hole on the holder
4. NOTE: minimize sample exposure as much as possible
   (a) This means:
      i. Breathe in when your face is close to the sample

ii. Unless necessary that it be uncovered (while screwing down the conductive clip for example), the sample should be covered by a lid

iii. Always hold the sample horizontally to the table top and face-up

5. Place the sample holder (still covered) on the imaging platform

6. Connect the sample BNC connector to the BNC leading into the input of the SR570 Current Preamplifier on top of the control box

   (a) This records electrical information from the sample and gets it to the AFM software

7. Connect the heater to the AFM environmental control so you can heat the sample the next day

8. Load tip holder into the head

9. Uncover the sample and place the head over it

A.1.2 Tuning Setup

1. Run normal AC topography tuning

   (a) Take thermal using get real (current tips we're using aren't in the system, must select custom tip and input length: 300 um, width:20 um, freq: 300 kHz for AD-42-AS)

   (b) Run the autotune with selected target amplitude

   (c) I've been using a target amplitude of 1V for autotuning with the AD-42-AS tips

A.1.3 AC Topography Scan

1. Engage with the sample

   (a) With a 1V target amplitude, a setpoint ranging from 730-750 mV has worked well for me (AD-42-AS), will sometimes go as low as 710 mV depending on imaging needs
   (b) If the engage is "sticky", lower the setpoint

2. Record all imaging parameters, especially set point and target amplitude
   (a) When you switch to KPFM through mode master, it will not save these values, but it will save all other imaging parameters
3. Remember to set the data path!
4. Set image parameters (scan size, rate, points & lines)
5. Begin scanning
6. Hunt around for a good charge injection flake–the flatter the better and the shorter the better, as shorter edges are easier to image over for Si vs MoS2 comparison
   (a) In my experience, flakes that look like a little speck of dust (maybe even with some see-through sections) are the best. Too opaque and the flake will often be really wrinkled.
   (b) Remember to use the zoom in function on the camera to be able to visually inspect flakes for quality before spending a lot of time imaging them

A.1.4 KPFM Test

1. Once you have found a viable flake for charge injection, switch to KPFM in Mode Master
2. Run the single force and electric tune to make sure they look normal for your tip.
3. Take a test KPFM image of your flake

(a) Helps make sure there are no pre-existing trapped charges/weird potential signals

A.1.5 Injection Test

1. Switch back to AC mode and take a quick topographic scan so that you have visual for doing a test injection

    (a) NOTE: Make sure to readjust your setpoint

2. Find a spot on the flake a little away from you intended imaging area to do a test charge injection

3. In the Master Panel under Imaging Mode, select “Contact”

4. Change your image base name for changing scanning techniques

5. In Master Panel select the Force tab at the top

6. In the Force tab select the Go There tab

7. Check on “Show Markers”, “Show Tip”, and “Withdraw During Movement”

8. Use the Go There, Pick Point, and Clear There controls to move the tip to where you would like to take your force curve

9. Leave the trigger point at 1V and trigger channel at DeflVolts

    (a) If you’re ever concerned about pushing too hard on the surface during injection, you can lower the trigger point

10. Click “Single Force”

    (a) This engages the tip with the surface until the deflection reaches 1V and then retracts the tip

11. Inspect the Single Force plot that is produced. If it looks like the one below in Figure A.1, you are ready to go. If you want to understand this plot more, read the AR Applications Guide on Force Curves in the section on ORCA

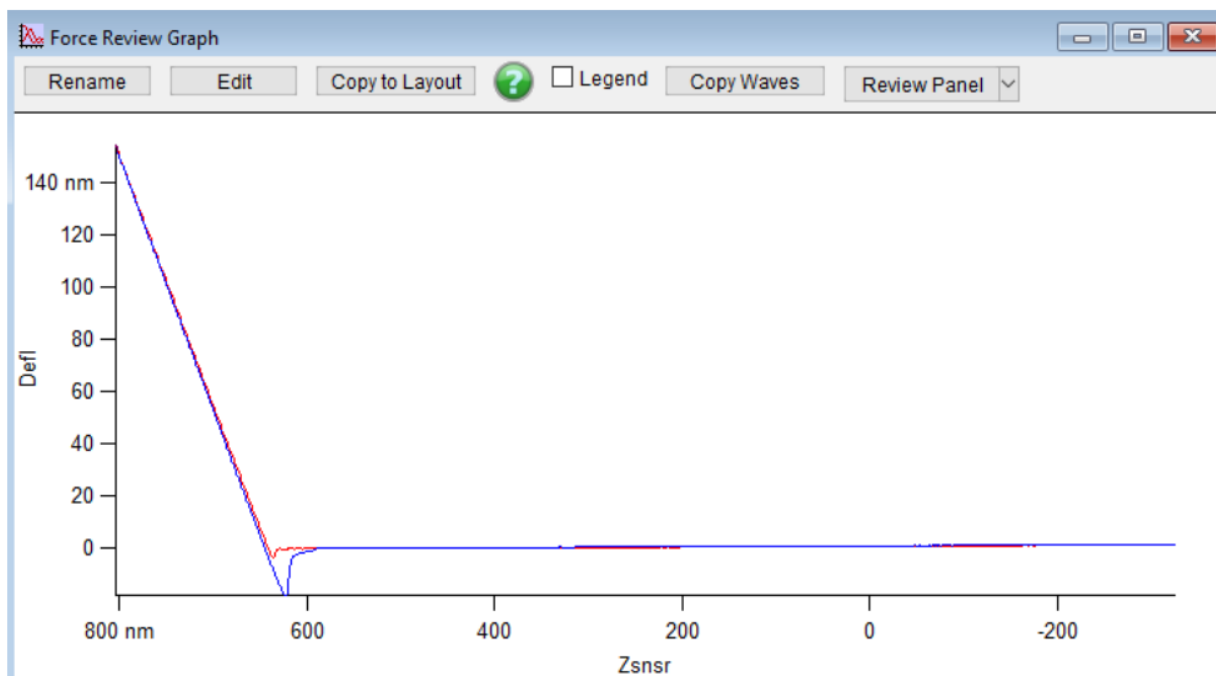

Figure A.1: Example deflection vs. z-sensor force curve.

(a) If your plot does not look like this, something is wrong with your tip-sample contact (likely that your tip is somehow too far away from the surface)

12. When ready to apply voltage move to the Misc tab in the Master Panel

13. Check box for "Bias Ramp after trigger".

14. Hit "Do IV Panel" button.

15. In this panel, you can control all aspects of the voltage application to the sample.

16. For the function, select "Function Editor" from the drop down menu.

17. In the function editor set up a 4V voltage hold.

(a) For the first segment, ramp the voltage from 0 V to 4 V in 0.1s

(b) Insert a second segment that holds from 4V to 4V for 120 s

(c) Insert a third segment that ramps down from 4V to 0 V in 0.1 s

18. Change "Drives What?" To "Tip Bias"

19. Turn on the SR570 Current Preamplifier on top of the control box.

20. Open the Channels panel from the Master Panel and enable the "UserIn0" channel (or whichever channel the sample electrical info is going to)

21. In the Sum & Deflection Meter, use the set up menu (button at bottom right of the panel) to select "UserIn0" and "TipBias" as channels to be displayed.

    (a) By seeing UserIn0 on the meter you can make sure that no significant current is being measured through the oxide.

22. When all is set up, hit "single force" to apply the voltage to the sample.

    (a) An error will pop up. Click yes and ignore.

A.1.6 Measure CPD

1. Switch back to KPFM through mode master.

    (a) Make sure to readjust your setpoint.

2. Measure the CPD for this injection using KPFM.

    (a) Decide based off the response if you think you need to switch tips, or if this tip and will yield viable results in nitrogen

    (b) If it's above 100 mV, you should be good

3. Set the tip and scan for imaging the next day if you are ready to go. Leave the laser on.

A.1.7 Flowing Nitrogen

1. Ensure the black membrane of the tip holder is flush with the sample holder.

2. Open the valve on the nitrogen tank.

3. Turn the black knob of the regulator open.

4. Further down the tubing for nitrogen flow to the enclosure, open the valve from the copper tubing to the plastic tubing.

    (a) There is a strong catch on this valve, ensure you actually open it past the catch.

5. Inside the enclosure, feel to make sure that nitrogen is flowing out of the plastic tubing ending.

6. Connect the two ends of plastic tubing (one coming into the enclosure, one attached to the sample holder) to begin nitrogen flow over the sample.

7. Go back to the tank and adjust the flow rate by adjusting the black knob on the flow rate meter. You want the silver bead around 45 and the black one around 110. These values are approximate and may vary slightly.

8. Record the tank pressure and time at the start of flowing nitrogen.

A.2 The Day of Imaging

A.2.1 Heating the Sample

1. Record the Nitrogen tank pressure.

2. Raise the head by turning the front wheel 5x clockwise.

3. Access the heating panel by:

(a) Opening the Programming menu (at the very top of the window)

(b) Choosing Cantilever Sample Holder from the drop down menu

(c) On the Cantilever Sample Holder panel, click the right hand tab at the top for sample holder

(d) Select the Poly Heater

(e) The temperature control menu should pop up on your screen

4. Clear the error message that it throws by clicking on "details" at the error section and then "clear" in the menu that pops up.

5. Turn the feedback on.

6. Select a heating speed of 90C/minute. Select a target temperature of 150C.

7. Click heating mode ON to begin heating.

8. You can open a live graph of the heater stage temperature by checking the "Collect Data" box and then hitting "more".

9. Once the sample reaches 150C, let it sit for 15 minutes.

10. After 15 minutes, set the target temperature to 70C for injection.

11. Once the sample reaches 70C, let it sit for five minutes to equilibrate.

12. After the equilibration period, retune and re-engage with the surface.

    (a) NOTE: The heater window may close when switching between imaging modes. You can reopen it the same way you accessed it the first time around.

A.2.2 Charge Injection

1. Take some topography scans, starting with a large one, to find your injection area. Things will have shifted during the heating process.
2. In the Master Panel under Imaging Mode, select “Contact”
3. Change your image base name for changing scanning techniques.
4. In Master Panel select the Force tab at the top
5. In the Force tab select the Go There tab
6. Check on “Show Markers”, “Show Tip”, and “Withdraw During Movement”. If “Show tip” and “show markers” are checked but they aren’t showing up, uncheck and recheck.
7. Use the Go There, Pick Point, and Clear There controls to move the tip to where you would like to take your force curve
8. Leave the trigger point at 1V and trigger channel at DeflVolts
    (a) If you’re ever concerned about pushing too hard on the surface during injection, you can lower the trigger point.
9. When ready to apply voltage, move to the Misc tab in the Master Panel
10. Check box for “Bias Ramp after trigger”
11. Hit “Do IV Panel” button
12. For the function, select “Custom Function” from the drop down menu.
13. In the function editor set up a 4V voltage hold.
    (a) For the first segment, ramp the voltage from 0 V to 4 V in 0.1s
    (b) Insert a second segment that holds from 4V to 4V for 120 s

(c) Insert a third segment that ramps down from 4V to 0 V in 0.1 s

14. Change Drives What? To “Tip Bias”

15. Turn on the SR570 Current Preamplifier on top of the control box

16. Open the Channels panel from the Master Panel and enable the “UserIn0” channel (or whichever channel the sample electrical info is going to)

17. In the Sum & Deflection Meter, use the set up menu (button at bottom right of the panel) to select “UserIn0” and “TipBias” as channels to be displayed.

    (a) By seeing UserIn0 on the meter you can make sure that no significant current is being measured through the oxide.

18. When all is set up, hit single force to apply the voltage to the sample

19. Use the controls in the Go There tab to move the tip to different spots for charge injection. The number of spots will depend on the exact details of your experiment.

A.2.3 Sample Heating II

1. Once charge injection is finished, raise the head off the sample by 2 turns of the front wheel.

2. Use the temperature control panel to heat the sample to 90C.

3. Once the sample is at 90C, let it equilibrate for five minutes.

4. After the equilibration period, retune and re-engage with the surface.

5. You will likely need to use AC topography at this time to relocate your injection spot, as things may have shifted during heating.

A.2.4 KPFM

1. Navigate to KPFM through the mode master
2. Rename your image base name if wanted
3. You will need to retune, both normal and electrical, and retake a force curve
    (a) Use your setpoint and target amplitude from AC topography
4. Remember to set an aggressive delta H (for this sample and tip, I've been fine with -25 nm to -30 nm).
5. Begin continuous scanning.
6. Periodically (maybe once an hour) retune the tip and retake the force curve between scans.

Bibliography

[1] "Molybdenum disulfide (MoS2) structure & properties."

[2] "MoS2 - molybdenum disulfide."

[3] D. Marinskiy, P. Edelman, J. Lagowski, T. C. Loy, C. Almeida, and A. Savtchouk, "Kelvin force microscopy and corona charging for semiconductor material and device characterization," vol. 99, pp. 13–23.

[4] S. Choudhary, D. Schwarz, H. S. Funk, R. Khosla, S. K. Sharma, and J. Schulze, "Impact of charge trapping on epitaxial p-ge$_{\text{-on-}}$ p-si and HfO_2 based al/HfO_2 /p-ge$_{\text{-on-}}$ p-si/al structures using kelvin probe force microscopy and constant voltage stress," vol. 20, pp. 346–355.

[5] M.-H. Zhang, "Electron trapping properties at HfO_2 /SiO_2 interface, studied by kelvin probe force microscopy and theoretical analysis," vol. 25, no. 8, p. 087701.

[6] "More things in heaven and earth: A celebration of physics at the millennium."

[7] B. G. Streetman and S. K. Banerjee, *Solid state electronic devices.* Always learning, Pearson, 7. ed., global ed ed.

[8] G. Bersuker, P. Zeitzoff, G. Brown, and H. R. Huff, "Dielectrics for future transistors," vol. 7, no. 1, pp. 26–33.

[9] G. D. Wilk, R. M. Wallace, and J. M. Anthony, "High- gate dielectrics: Current status and materials properties considerations," vol. 89, no. 10, pp. 5243–5275.

[10] S. Zhang, T. Zhang, H. Yu, T. Li, X. Li, C. Cui, Y. Zhou, H. Guo, S. Wang, D. Zheng, L. Huang, L. Bai, S. Liu, C. Shen, W. Yang, L. Du, D. Shi, L. Xian, X. Tao, Y. Chai, N. Li, and G. Zhang, "Wafer-scale high- HfO2 dielectric films with sub-5-Å equivalent oxide thickness for 2d MoS2 transistors," vol. 17, no. 1, p. 1888.

[11] Z. Liu, Q. Mao, V. Kamboj, R. Kothari, P. Miller, K. Reidy, A. C. T. Van Duin, R. Jaramillo, and F. M. Ross, "Epitaxial formation of ultrathin HfO_2 on multilayer graphene by sequential oxidation," vol. 19, no. 27, pp. 25028–25041.

[12] A. Paul, G. Kumar, A. Das, G. Larrieu, and S. De, "Hafnium oxide-based ferroelectric field effect transistors: From materials and reliability to applications in storage-class memory and in-memory computing," vol. 138, no. 1, p. 010701.

[13] "Celano 2019 book electrical atomic force microscopy for nanoelectronics.pdf."

[14] J. Chen, M.-Y. Sun, Z.-H. Wang, Z. Zhang, K. Zhang, S. Wang, Y. Zhang, X. Wu, T.-L. Ren, H. Liu, and L. Han, "Performance limits and advancements in single 2d transition metal dichalcogenide transistor," vol. 16, no. 1, p. 264.

[15] F. Zheng, W. Meng, and L.-J. Li, "Continue the scaling of electronic devices with transition metal dichalcogenide semiconductors," vol. 25, no. 10, pp. 3683–3691.

[16] C. Patra, S. Mondal, R. Mukherjee, and Y. Nandakishora, "Advanced synthesis and unique properties of 2d transition metal dichalcogenides for realizing next-generation applications," vol. 5, no. 5, pp. 745–766.

[17] Z. Sun, C.-S. Pang, P. Wu, T. Y. Hung, M.-Y. Li, S. L. Liew, C.-C. Cheng, H. Wang, H.-S. P. Wong, L.-J. Li, I. Radu, Z. Chen, and J. Appenzeller, "Statistical assessment of high-performance scaled double-gate transistors from monolayer WS_2," vol. 16, no. 9, pp. 14942–14950.

[18] H. Wan, W. Li, X. Ma, Y. Mu, G. Xie, M. Li, B. Guo, and J. R. Gong, “3 nm channel MoS_2 transistors by electromigration of metal interconnection,” vol. 5, no. 1, pp. 247–254.

[19] T. Ishihara, Y. Nakasaki, D. Matsushita, K. Tatsumura, and K. Kato, “Interface defect engineering for high-performance MOSFETs with novel carrier mobility model: Theory and experimental verification,” vol. 10, no. 5, p. 055020.

[20] Y.-C. Lin, R. Torsi, R. Younas, C. L. Hinkle, A. F. Rigosi, H. M. Hill, K. Zhang, S. Huang, C. E. Shuck, C. Chen, Y.-H. Lin, D. Maldonado-Lopez, J. L. Mendoza-Cortes, J. Ferrier, S. Kar, N. Nayir, S. Rajabpour, A. C. T. Van Duin, X. Liu, D. Jariwala, J. Jiang, J. Shi, W. Mortelmans, R. Jaramillo, J. M. J. Lopes, R. Engel-Herbert, A. Trofe, T. Ignatova, S. H. Lee, Z. Mao, L. Damian, Y. Wang, M. A. Steves, K. L. Knappenberger, Z. Wang, S. Law, G. Bepete, D. Zhou, J.-X. Lin, M. S. Scheurer, J. Li, P. Wang, G. Yu, S. Wu, D. Akinwande, J. M. Redwing, M. Terrones, and J. A. Robinson, “Recent advances in 2d material theory, synthesis, properties, and applications,” vol. 17, no. 11, pp. 9694–9747.

[21] P. Wiśniewski, P. Jeżak, and M. Jarosik, “Analysis of charge-trapping effects in ultra-low current metal–oxide–semiconductor–oxide–semiconductor devices,” vol. 15, no. 9, p. 095304.

[22] H.-W. You and W.-J. Cho, “Charge trapping properties of the HfO2 layer with various thicknesses for charge trap flash memory applications,” vol. 96, no. 9, p. 093506.

[23] C. Mannequin, P. Gonon, C. Vallée, A. Bsiesy, H. Grampeix, and V. Jousseaume, “Dielectric relaxation in hafnium oxide: A study of transient currents and admittance spectroscopy in HfO2 metal-insulator-metal devices,” vol. 110, no. 10, p. 104108.

[24] A. Ranjan, N. Raghavan, K. Shubhakar, R. Thamankar, J. Molina, S. J. O’Shea, M. Bosman, and K. L. Pey, “CAFM based spectroscopy of stress-induced defects in

HfO2 with experimental evidence of the clustering model and metastable vacancy defect state," in *2016 IEEE International Reliability Physics Symposium (IRPS)*, pp. 7A–4–1–7A–4–7, IEEE.

[25] A. Ranjan, S. J. O'Shea, M. Bosman, N. Raghavan, and K. L. Pey, "Localized probing of dielectric breakdown in multilayer hexagonal boron nitride," vol. 12, no. 49, pp. 55000–55010.

[26] H. O. Jacobs and A. Stemmer, "Measuring and modifying the electric surface potential distribution on a nanometre scale: a powerful tool in science and technology," vol. 27, no. 5, pp. 361–367.

[27] P. Kumar, R. Khosla, and S. K. Sharma, "Nanoscale investigations: Surface potential of rare-earth oxide (re2o3) thin films by kelvin probe force microscopy for next generation CMOS technology," vol. 4, pp. 69–76.

[28] R. Kumar, P. Gupta, and S. K. Sharma, "Nanoscale probing of surface charges in functional copper-metal organic clusters by kelvin probe force microscopy for field-effect transistors," vol. 8, no. 20, p. 2100529.

[29] R. Khosla, E. G. Rolseth, P. Kumar, S. S. Vadakupudhupalayam, S. K. Sharma, and J. Schulze, "Charge trapping analysis of metal/al_2 o_3 /SiO_2 /si, gate stack for emerging embedded memories," vol. 17, no. 1, pp. 80–89.

[30] Yulong Han, Zongliang Huo, Xinkai Li, Guoxing Chen, Xiaonan Yang, Dong Zhang, Yong Wang, Tianchun Ye, and Ming Liu, "Investigation of charge loss mechanism of thickness-scalable trapping layer by variable temperature kelvin probe force microscopy," vol. 34, no. 7, pp. 870–872.

[31] C. Zhu, Z. Xu, Z. Huo, R. Yang, Z. Zheng, Y. Cui, J. Liu, Y. Wang, D. Shi, G. Zhang, F. Li, and M. Liu, "Investigation on interface related charge trap and loss characteristics

of high-k based trapping structures by electrostatic force microscopy," vol. 99, no. 22, p. 223504.

[32] J. Wang, H. Zhang, G.-s. Cao, L.-h. Xie, and W. Huang, "Injection and retention characterization of trapped charges in electret films by electrostatic force microscopy and kelvin probe force microscopy," vol. 217, no. 20, p. 2000190.

[33] E. V. Dementeva, P. A. Dementev, M. A. Yagovkina, and M. V. Zamoryanskaya, "Determination of type and concentration of traps in nanoscale-thick HfO_2 films applicable for gate dielectric stacks," vol. 6, no. 18, pp. 16212–16220.

[34] C. Y. Ng, T. P. Chen, H. W. Lau, Y. Liu, M. S. Tse, O. K. Tan, and V. S. W. Lim, "Visualizing charge transport in silicon nanocrystals embedded in SiO2 films with electrostatic force microscopy," vol. 85, no. 14, pp. 2941–2943.

[35] M. S. Dunaevskiy, P. A. Alekseev, P. Girard, E. Lahderanta, A. Lashkul, and A. N. Titkov, "Kelvin probe force gradient microscopy of charge dissipation in nano thin dielectric layers," vol. 110, no. 8, p. 084304.

[36] N. Knorr, S. Rosselli, and G. Nelles, "Surface-potential decay of biased-probe contact-charged amorphous polymer films," vol. 107, no. 5, p. 054106.

[37] "Plasma-enhanced ALD (PE-ALD)."

[38] C. Villeneuve-Faure, L. Boudou, K. Makasheva, and G. Teyssedre, "Atomic force microscopy developments for probing space charge at sub-micrometer scale in thin dielectric films," vol. 23, no. 2, pp. 713–720.

[39] S. Yoon, S. Choi, M.-H. Lee, S. Kim, S. Jang, H. Park, D. Lee, S.-Y. Yang, and J. Y. Park, "Nanoscale dynamics of buried charge trap in oxide-nitride-oxide stacks investigated using kelvin probe force microscopy," vol. 25, no. 42, pp. 15256–15263. _eprint: https://doi.org/10.1021/acs.nanolett.5c03652.

[40] P. González-Izquierdo, N. Rochat, M. Charles, T. Sochacki, and Borowik, "Kelvin probe force microscopy ender variable illumination: A novel technique to unveil charge carrier dynamics in gan," vol. 127, pp. 12727–12734. $_eprint : https : //doi.org/10.1021/acs.jpcc.3c01887$.